

Review

Battery-Type Transition Metal Oxides in Hybrid Supercapacitors: Synthesis and Applications

Bikash Raut ¹, Md. Shahriar Ahmed ¹, Hae-Yong Kim ², Mohammad Mizanur Rahman Khan ³ , Gazi A. K. M. Rafiqul Bari ³ , Mominul Islam ^{1,*}  and Kyung-Wan Nam ^{1,*} 

¹ Department of Energy & Materials Engineering, Dongguk University, Seoul 04620, Republic of Korea; 2023121093@dgu.ac.kr (B.R.); shahriar.emcl@dgu.ac.kr (M.S.A.)

² Department of Advanced Battery Convergence Engineering, Dongguk University, Seoul 04620, Republic of Korea

³ School of Mechanical Smart and Industrial Engineering, Gachon University, Gyeonggi-do 13120, Republic of Korea; mmrkhan@gachon.ac.kr (M.M.R.K.); grafiqulbari@gachon.ac.kr (G.A.K.M.R.B.)

* Correspondence: mobin85@dongguk.edu (M.I.); knam@dongguk.edu (K.-W.N.); Tel.: +82-2-2260-4978 (K.-W.N.)

Abstract: Hybrid supercapacitors (HSCs) have garnered growing interest for their ability to combine the high energy storage capability of batteries with the rapid charge–discharge characteristics of supercapacitors. This review examines the evolution of HSCs, emphasizing the synergistic mechanisms that integrate both Faradaic and non-Faradaic charge storage processes. Transition metal oxides (TMOs) are highlighted as promising battery-type electrodes owing to their notable energy storage potential and compatibility with various synthesis routes, including hydro/solvothermal methods, electrospinning, electrodeposition, and sol–gel processes. Particular attention is directed toward Ti-, Co-, and V-based TMOs, with a focus on tailoring their properties through morphology control, composite formation, and doping to enhance electrochemical performance. Overall, the discussion underscores the potential of HSCs to meet the growing demand for next-generation energy storage systems by bridging the gap between high energy and high power requirements.



Academic Editors: Changzhou Yuan, Xianzhong Sun and Xiong Zhang

Received: 30 December 2024

Revised: 27 January 2025

Accepted: 3 February 2025

Published: 5 February 2025

Citation: Raut, B.; Ahmed, M.S.;

Kim, H.-Y.; Rahman Khan, M.M.; Bari, G.A.K.M.R.; Islam, M.; Nam, K.-W.

Battery-Type Transition Metal Oxides in Hybrid Supercapacitors: Synthesis and Applications. *Batteries* **2025**, *11*, 60. <https://doi.org/10.3390/batteries11020060>

Copyright: © 2025 by the authors.

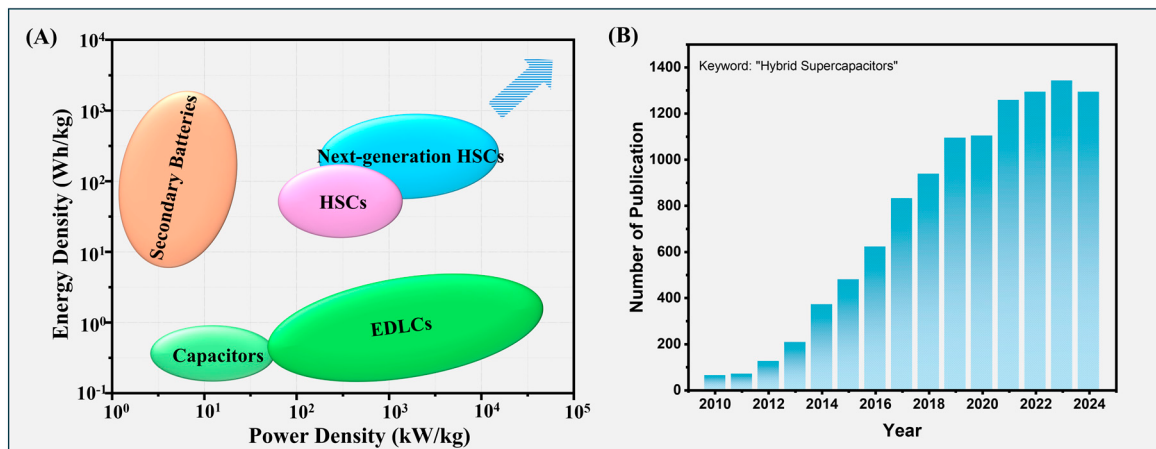
Licensee MDPI, Basel, Switzerland.

This article is an open access article distributed under the terms and conditions of the Creative Commons Attribution (CC BY) license (<https://creativecommons.org/licenses/by/4.0/>).

1. Introduction

The rapid depletion of non-renewable energy sources, such as fossil fuels, and the alarming rise in environmental pollution caused by their extensive use have spurred the development of renewable energy alternatives in recent years [1,2]. Technologies such as solar energy, electrochemical energy storage (including batteries and supercapacitors), and hydrogen energy have gained significant attention. Among various electrochemical energy storage systems (EES), batteries and supercapacitors stand out as the most promising devices [3–7]. The high specific capacity and energy density of secondary batteries, attributed to bulk redox reactions, position them at the top end of the energy density axis on the Ragone plot; a graphical tool that compares the energy density and power density of various energy storage systems including batteries, supercapacitors and hybrid supercapacitors in terms of both how much energy they can store and how quickly they can deliver that energy [8–10] as shown in Scheme 1A. The high energy density of batteries ($150\text{--}300 \text{ WhKg}^{-1}$) enables long driving range for EVs [11]. But when it comes to power density (below 350 Wkg^{-1}), batteries have inferior power density [12,13]. The power

density on the other hand in the case of supercapacitors is high but supercapacitors have very low energy density, almost 10 times lower than that of batteries, so, it is practically not feasible to use supercapacitors where high energy density is required [14–17]. As both high energy density and high power density are critical for advanced energy storage systems, there is a growing need to develop energy materials capable of delivering both simultaneously. In the context of the Ragone plot, which visually maps the trade-off between energy density and power density, and balance between these two-performance metrics. One promising class of energy materials that has attracted extensive research attention is hybrid supercapacitors (HSCs) [18]. HSCs are innovative energy storage devices that combine the advantages of battery-like materials (Faradaic redox reactions) with supercapacitor-like materials (non-Faradaic double-layer capacitance) [19]. This hybridization enables HSCs to bridge the gap between two extremes of the Ragone plot, batteries, which provide high energy density but suffer from low power density, and supercapacitors, which offer high power density but exhibit limited energy density. By leveraging the complementary mechanisms of batteries and supercapacitors, HSCs open up new and previously unexplored regions of the Ragone plot [1,20]. The battery-like component of HSCs contributes to higher energy storage through Faradaic redox reactions, where energy is stored in the bulk of the active material via ion insertion/extraction processes or conversion, and alloying processes. Simultaneously, the supercapacitor-like component facilitates rapid charge/discharge capability, delivering high power density through surface-based, non-Faradaic charge storage mechanisms. This dual nature of HSCs enables a unique synergy that addresses the inherent limitations of both batteries and supercapacitors, providing a balance between fast energy delivery and large energy storage capacity. Due to these advantages, hybrid supercapacitors are emerging as a key technology for next-generation energy storage systems, garnering significant research focus globally. Over the past decade, the field has witnessed exponential growth, with a substantial increase in the number of publications each year, reflecting the increasing interest and progress in this area as shown in Scheme 1B. This trend underscores the potential of HSCs to revolutionize energy storage by simultaneously enhancing both energy and power performance. Ongoing innovations in material design, electrode architecture, and device engineering are driving the next generation of HSCs by enhancing both energy and power densities, thereby offering more efficient and versatile energy storage solutions.



Scheme 1. (A) Ragone plots for secondary batteries, supercapacitors, and HSCs. (B) Publication numbers over time.

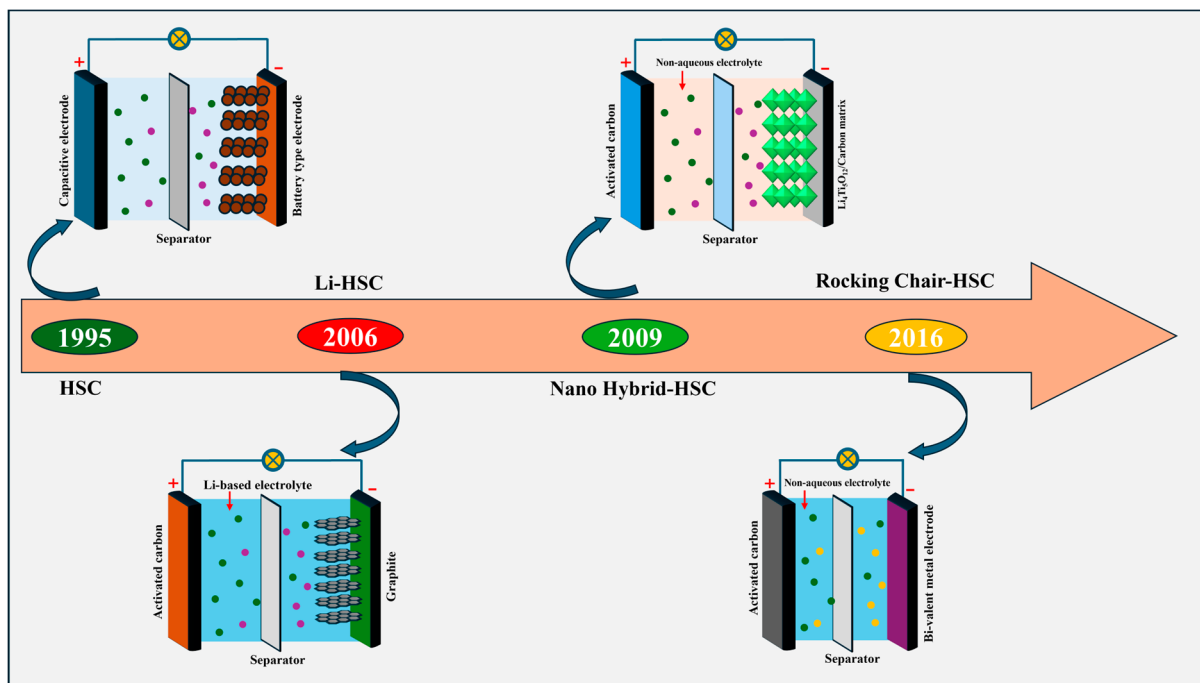
Transition metal oxides (TMOs) have emerged as a pivotal class of materials in the development of hybrid supercapacitors (HSCs) due to their remarkable redox activity, high

theoretical capacitance, and tunable electronic properties [21–24]. Their ability to facilitate Faradaic charge storage mechanisms enables them to deliver energy densities comparable to batteries while retaining the power capabilities of supercapacitors. This dual functionality makes them indispensable for next-generation energy storage technologies aimed at addressing the growing demand for efficient, sustainable, and versatile energy solutions. Previous reviews have extensively covered TMO fundamentals and their electrochemical properties [1,18,20,25]. In contrast, this review provides a comprehensive overview of fundamentals and history of HSCs, detailed analysis of the diverse TMOs used as battery-type electrodes, including oxides of vanadium, cobalt, and titanium. Special attention is given to the influence of their crystalline structure, oxidation states, and defect chemistry on their electrochemical behavior. These factors play a critical role in determining the charge storage capacity, rate capability, and long-term stability of HSC systems. Furthermore, this article delves into state-of-the-art synthesis techniques such as sol–gel, hydrothermal, electrospinning, and electrodeposition methods. These methods enable precise control over the morphology, particle size, and surface area of TMOs, which are crucial for optimizing their interaction with electrolytes. Recent advancements in nanostructuring strategies, including the development of hierarchical architectures and composite materials, are discussed for their ability to enhance ion diffusion and electronic conductivity. The review also addresses key challenges in the application of TMOs in HSCs, such as cyclic stability, and conductivity limitations. Emerging solutions, including doping strategies, and hybridization with carbon-based materials are critically evaluated for their effectiveness in overcoming these challenges. Finally, this review outlines future directions for research and development in this field, emphasizing the need for scalable synthesis techniques, environmentally friendly production methods, and the integration of TMOs into flexible and wearable energy storage devices. By bridging the performance gap between batteries and supercapacitors, TMOs hold the potential to revolutionize energy storage systems and pave the way for sustainable technological advancements.

2. History

The early history of HSCs, where two electrodes combine to form a new hybridized device, can be traced back to the mid-1990s. In 1995, Aleksei Stepanov et al. reported the successful hybridization of a nickel oxide electrode and a fibrous carbonic material to form a hybrid device with enhanced capacity compared to the bare double-layer capacitor [26]. This hybridization of two different types of materials to create a new device with enhanced electrochemical properties opened up a new door for the exploration of hybrid devices. The possibility of hybridization of two materials either similar or different (symmetric and asymmetric) allows researchers to explore various combinations to make hybrid devices with different working mechanisms on either side of the electrodes. A timeline of other types of hybrid devices is presented in Scheme 2. In 2006, Aida et al. reported a Li-based hybrid supercapacitor using carbon-based electrodes and Li-based non-aqueous electrolytes. The non-aqueous Li-based electrolyte coupling with carbon-based electrodes enhanced the energy output of the hybrid system by increasing the operational potential window [27]. The hybridization of composite-type negative electrodes with carbon-based positive electrodes with a non-aqueous electrolyte was reported by Naoi et al. in 2009. A nanocomposite of lithium titanate ($\text{Li}_4\text{Ti}_5\text{O}_{12}$; LTO) with carbon nanofiber (CNF) was used as a negative electrode and hybridized with an activated carbon electrode to obtain a hybrid supercapacitor, which was termed a nano-hybrid supercapacitor (NHSC) or nano-hybrid capacitor (NHC). The zero-strain ion insertion capability of LTO allows an insertion-type redox mechanism in LTO/CNF composite electrodes without significant volume change during the process. Also, the operational potential window of LTO lies in between the

decomposition limit of traditional non-aqueous-based electrolytes which eliminates the possibility of electrolyte decomposition and unwanted side reaction-based non-reversible capacity contribution [28,29]. In 2016, Yoo et al. reported an HSC with “rocking-chair”-type mechanism. The HSC was comprised of di-valent metal negative electrode, activated carbon positive electrode and a non-aqueous electrolyte. This new “rocking-chair” type mechanism enhances the energy density of the HSC and lowers the volume of required electrolytes in the HSC system [30].



Scheme 2. Timeline of different types of HSCs.

3. Fundamental Concepts of HSC

Before delving into the concepts behind the HSCs, it is essential to understand their two components, i.e., batteries and supercapacitors. Batteries and supercapacitors both are charge storage systems with different electrochemical charge storage mechanisms, the former stores charge based on bulk Faradaic processes, and the latter is based on near-surface non-Faradaic processes [31–34]. The bulk redox process of batteries results in high energy density, but low power density stems from the sluggish ionic diffusion (diffusion limitation). On the other hand, supercapacitors possess low energy density due to the absence of redox reactions and high power density resulting from fast ionic transport without significant diffusion limitations. As both have different charge storage mechanisms, they can be distinguished by cyclic voltammograms. For instance, due to the involvement of redox reactions clear well-separated anodic (oxidation) and cathodic (reduction) peaks are visible in cyclic voltammograms of batteries, for supercapacitors, these clear cathodic-anodic peaks are missing, and rectangular-shaped voltammograms can be seen stemming from non-Faradaic processes [35,36]. The mechanism of these two energy storage systems can be obtained from sweep voltammetry, like, whether the process is diffusion controlled (like in batteries) or diffusion independent (supercapacitors). For an electrochemical process, the following equation provides insight into the charge storage mechanism of the electrochemical system [37,38]:

$$i = av^b \quad (1)$$

Here, i is the peak current, v is the sweep rate, and b is a variable, which can be obtained from the slope of the logarithmic plot between i and v . The value of $b = 0.5$ indicates battery-like diffusion-controlled redox processes and this can be expressed as a square root relationship between peak current and sweep rate by Equation (2):

$$i = a \sqrt{v} \quad (2)$$

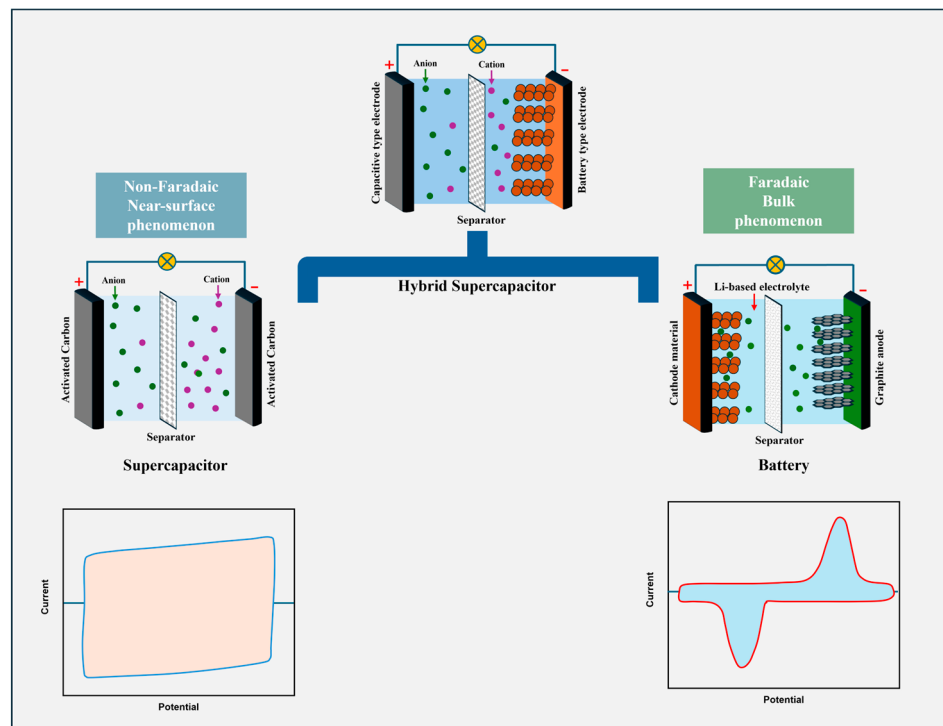
For a capacitive process (supercapacitor-like), the peak current is linearly related to the sweep rate, i.e., $b = 1$, and can be expressed by Equation (3):

$$i = av \quad (3)$$

We can combine these two charge storage mechanisms in a single system to obtain a cumulative effect on electrochemical performance compared to its single components, i.e., hybrid supercapacitors (HSCs). This hybridization can solve the low power-density issue of batteries and the low energy-density issue of supercapacitors by utilizing both Faradaic and non-Faradaic reactions. So, for HSC, we can expect the value of b between 0.5 and 1 ($0.5 < b < 1$) from Equations (1) and (2), and this can be expressed as the linear combination of both equations as follows [39,40]:

$$i(HSC) = a\sqrt{v} + av \quad (4)$$

The hybridization of battery-like and supercapacitor-like components to form a hybrid supercapacitor system with their cyclic voltammograms is shown schematically in Scheme 3.



Scheme 3. Hybridization of battery and supercapacitor type electrodes to hybrid supercapacitor.

4. Transition Metal Oxides as Battery-Type Electrodes

Transition metal oxides are emerging as a new paradigm in energy-related applications owing to their unique properties. This review delves into the important role of transition metal oxides (TMO) as battery-type electrodes in hybrid supercapacitor (HSC) systems,

highlighting their unique electrochemical properties and potential to bridge the gap between batteries and capacitors. Additionally, it explores the various synthesis techniques employed to tailor their structure, composition, and performance, offering insights into advancements and challenges in this dynamic field.

5. Synthesis of TMOs

5.1. Hydro/Solvothermal

Hydro/solvothermal synthesis is one of the most popular, scalable, simple, and cost-effective synthesis techniques. In this technique reaction is carried out in a sealed vessel such as an autoclave, to create a high-pressure and high-temperature environment. High pressure and temperature inside the autoclave facilitate chemical reactions and material formation. Hydrothermal and solvothermal both work on this same principle just with the assistance of different solvents, in hydrothermal, water is used as a solvent, and in solvothermal other solvents like alcohols, amines, or glycerol's are used as solvents for the dissolution of precursors. A schematic of the hydrothermal synthesis process is shown in Figure 1A. In hydrothermal synthesis depending upon reactant ratio, synthesis temperature, and synthesis time, products with different morphologies and functionalities can be obtained, which makes it an important synthesis technique to synthesize different materials including battery-type TMOs. For instance, MnO_2 nanowires [41], MgCo_2O_4 nanoflakes [42], FeCo_2O_4 nanoflakes [43], and Mn_3O_4 nanorods [44] were synthesized utilizing hydrothermal synthesis. The solvothermal method is also used to synthesize oxides like $\text{MnCo}_2\text{O}_{4.5}$ with pod-like microstructure [45]. The hydro/solvothermal technique is also used to synthesize composite materials. Recently, Yu and colleagues synthesized $\text{ZnMoO}_4/\text{MoO}_3$ composite materials by hydrothermal method [46]. Other composites like $\text{Cu}_2\text{O}-\text{CuO}$ -reduced graphene oxide (RGO) [47] and $\text{ZnO}@\text{Fe}_2\text{O}_3$ [48] were also synthesized using this synthesis method.

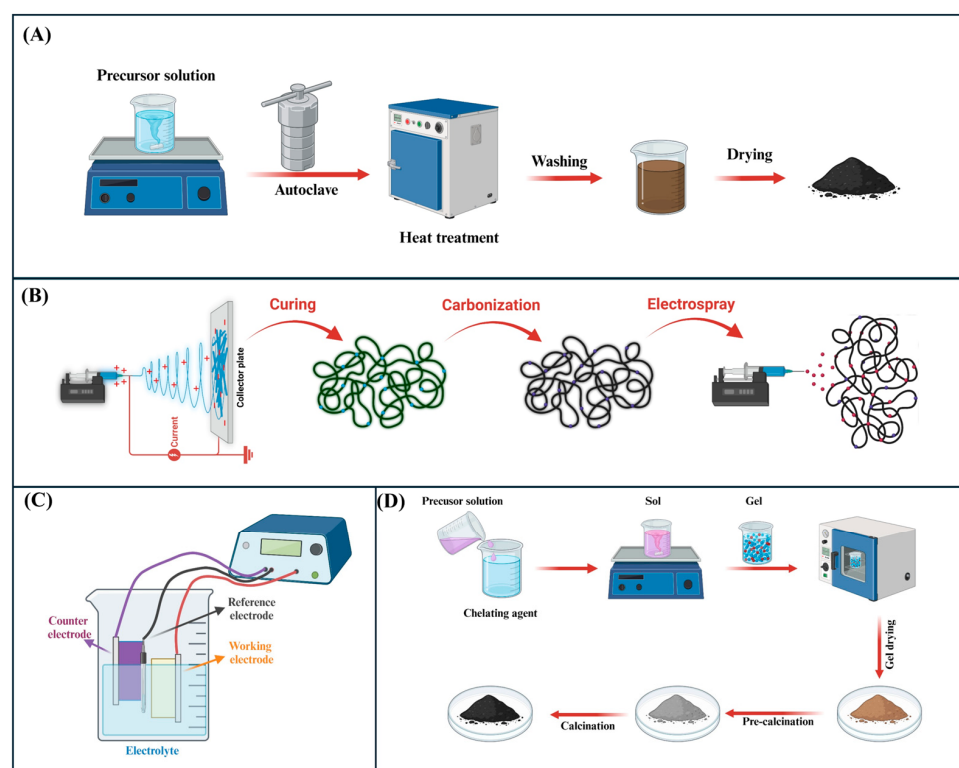


Figure 1. Schematic of different synthesis techniques. (A) Hydro/solvothermal. (B) Electrospraying. (C) Electrodeposition. (D) Sol–gel. Images created by BioRender.com.

5.2. Electrospinning

Electrospinning is a versatile and efficient method for fabricating ultrafine fibers. It is a simple and effective technique for producing continuous fibers at the micro- and nanoscale from a polymer solution or melt under the influence of a high-voltage electric field [49]. The method is known for its ability to fabricate fibers with high surface area, fine diameters, and controlled morphology. This electrospinning technique can be utilized to synthesize transition metal oxide nanofibers with several benefits such as self-standing electrodes with no requirement of binders, high surface area, enhanced electron transport, and enhanced stability [50]. These benefits motivated researchers to utilize this technique to synthesize TMOs for several applications including energy applications. For instance, Cao et al. synthesized a series of $\text{La}_x\text{Sr}_{1-x}\text{NiO}_{3-\delta}$ ($0.3 \leq x \leq 1$) nanofibers using an electrospinning technique [51]. Several other TMOs, hierarchical Co_3O_4 [52], MgCo_2O_4 nanofibers [53], ZnFe_2O_4 nanofibers [54], porous-high aspect ratio- Mn_3O_4 nanofibers [55], and coaxial-cable-like Mn_2O_3 nanofibers [56] were also fabricated using electrospinning technique and utilized in energy applications. In 2019, Xu et al. reported the synthesis of a core–shell $\text{NiCo}_2\text{O}_4\text{-C@Ni(OH)}_2$ nanofibers using the electrospinning technique, which also proves the versatility of the electrospinning technique to synthesize structurally different TMO nanofibers [57]. A schematic of the electrospinning process is shown in Figure 1B, the versatility of the electrospinning method to couple with techniques like electrospraying to synthesize composite TMOs is also shown schematically.

5.3. Electrodeposition

Electrodeposition or electrochemical deposition is another versatile and cost-effective technique for fabricating TMO-based electrode materials with controlled properties like morphology, thickness, and composition. In this technique, an electric potential is used to deposit the intended material from its precursor solution on a conductive electrode surface like carbon fibers, stainless steel, and nickel foam. Depending on the charges of the substrate on which electrodeposition was performed, it can be divided into cathodic (negatively charged) and anodic (positively charged) electrodeposition. A wide range of TMOs are fabricated with this technique, with controlled composition, morphology, and thickness, and proper optimization of solution pH, applied potential, and precursor ratio [58]. For instance, Joo and co-workers electrodeposited porous and amorphous CuO film on a stainless-steel substrate by cathodic electrodeposition using copper sulfate solution with an optimized pH of 9.0 and an applied potential of 1.05 V vs. saturated calomel electrode (SCE) [59]. Several other TMOs were also fabricated using this electrodeposition technique, like $\alpha\text{-MnO}_2$ [60], MnO_2 nanowires [61], V_2O_5 [62], NiO [63], MnCo_2O_4 nanosheets [64], 3D mesoporous Fe_2O_3 [65] and Co_3O_4 nanoflakes [66] were electrodeposited on different substrates. A schematic of the electrodeposition process is shown in Figure 1C.

5.4. Sol–Gel

The sol–gel method is a widely used wet-chemical synthesis technique for synthesizing inorganic materials such as transition metal oxides. Sol–gel is a bottom-up synthesis technique that involves transforming a liquid “sol” of precursors into a solid “gel” network, which is then processed to obtain the final material [67]. Figure 1D schematically shows the detailed synthesis process. The sol–gel approach offers several notable advantages, including uniform mixing at the molecular level (ensuring high homogeneity), broad versatility in material design, and precise control over structural features [68]. This technique has been used to synthesize various TMOs, such as spinel Co_3O_4 [69], NiCo_2O_4 [70,71], FeCo_2O_4 [72], MnO_2 nanowires [73], and composite $\text{LaNiO}_3/\text{NiO}$ [74].

6. TMOs as Battery-Type Electrodes for HSC

6.1. Ti-Based TMOs

Relying on high natural abundance, chemical stability, cost-effectiveness, and excellent safety, Ti-based oxide materials such as TiO_2 and $\text{Li}_4\text{Ti}_5\text{O}_{12}$ are widely used as electrode materials for supercapacitors and secondary battery applications, such as anodes in Li and Na-ion batteries [75,76].

6.1.1. TiO_2

The most abundant oxide of titanium, TiO_2 exists in four major polymorphs in nature, including rutile, anatase, brookite, and TiO_2 (B) as shown in Figure 2A [77]. Most of these polymorphs exhibit intrinsically low electrical conductivity except TiO_2 (B), which possesses higher electrical conductivity compared to other polymorphs. Because of its good electrical conductivity, TiO_2 (B) is used as an anode for Li-ion batteries (LIBs) and Li-ion capacitors (LICs) without further modification like carbon coating or nanocomposites with other conducting materials [78,79]. Wang et al. reported the successful fabrication of an HSC using TiO_2 (B) nanowires as an anode and carbon nanotube (CNT) as a cathode with enhanced energy density, power density, and cycling stability, higher than CNT-CNT symmetric supercapacitors [80]. However, while TiO_2 (B) resolves the conductivity issue compared to other TiO_2 polymorphs, it is more structurally complex and can be challenging to synthesize in large quantities with uniform morphologies. In addition, despite its relatively higher conductivity, TiO_2 (B) still falls short of ideal metallic or graphitic levels, sometimes necessitating further optimization through doping or carbon integration for applications requiring ultrahigh power densities. Scale-up and cost also remain considerations: bulk production of phase-pure TiO_2 (B) may require carefully controlled synthesis routes that can drive up manufacturing expenses. On the other hand, due to intrinsic low electrical conductivity, other polymorphs of TiO_2 are mostly used as composites with carbon or other functional materials. For instance, Kang and co-workers reported the fabrication of an HSC utilizing an anatase TiO_2 -RGO composite anode paired with an activated carbon (AC) cathode. The HSC device with TiO_2 -RGO anode exhibited enhanced electrochemical performance compared to the HSC device having a synthesized TiO_2 -without RGO and a commercial TiO_2 [81]. A critical drawback here is that integrating carbon (e.g., reduced graphene oxide, carbon nanotubes) or other conductive phases adds to the complexity of material synthesis and can introduce additional costs for large-scale production. Moreover, achieving a uniform dispersion of carbon within TiO_2 is essential for stable long-term performance, and any agglomeration could lead to localized conductivity issues. Reproducibility is also a key concern, especially for industrial-scale applications, where large batch sizes must maintain consistent phase composition and particle size distribution. To address the intrinsic issues of TiO_2 , Ramasubbu et al. explored morphologically different TiO_2 . They reported the successful synthesis of 3D porous TiO_2 aerogel/Cobalt-metal-organic framework (TiO_2 aerogel/Co-MOF) composites using sol-gel method and used as a battery-type electrode to fabricate an HSC device [82]. The TiO_2 aerogel and Co-MOF synergistically enhanced the contact between electrolyte and electrode interface, increased the electroactive sites for Faradaic reactions, decreased the internal resistance. TiO_2 aerogel/Co-MOF composite also enhanced the ionic transportation by shortening the diffusion path and improved the mechanical stability of the composite electrode. The HSC fabricated using TiO_2 aerogel/Co-MOF as battery-type electrode and activated carbon (AC) as capacitive electrode (as shown in Figure 2B) shows enhanced electrochemical performance. The fabricated HSC shows an enhanced specific capacity of $111.2 \text{ C}\cdot\text{g}^{-1}$ at a current density of $0.8 \text{ A}\cdot\text{g}^{-1}$ and a high specific power density of $1875 \text{ W}\cdot\text{kg}^{-1}$, which is greater than bare TiO_2 aerogel and other TiO_2 /carbon composites without Co-MOF. The AC and

TiO₂ aerogel/Co-MOF electrodes operate at different potential windows and therefore for the HSC device, combination of these two potential windows can be expected, which leads to the enhancement of workable potential window of 1.5 V (as shown in Figure 2C(a)). The battery and supercapacitor-like behavior of the HSC device arising from different energy storage mechanisms (Faradaic and non-Faradaic) is evident from the broad peaks and rectangular shape of the CV curves as can be seen in Figure 2C(b). The distorted triangular shape and small plateau in the GCD curve also confirm the HSC-like behavior (as shown in Figure 2C(c)). The fabricated HSC device shows long-term cycling stability. When cycling the HSC at a current density of 2 A·g⁻¹ for 5000 cycles, it shows 93% of capacity retention (as shown in Figure 2C(d)). Other TiO₂ composites were also reported as an anode for HSC applications.

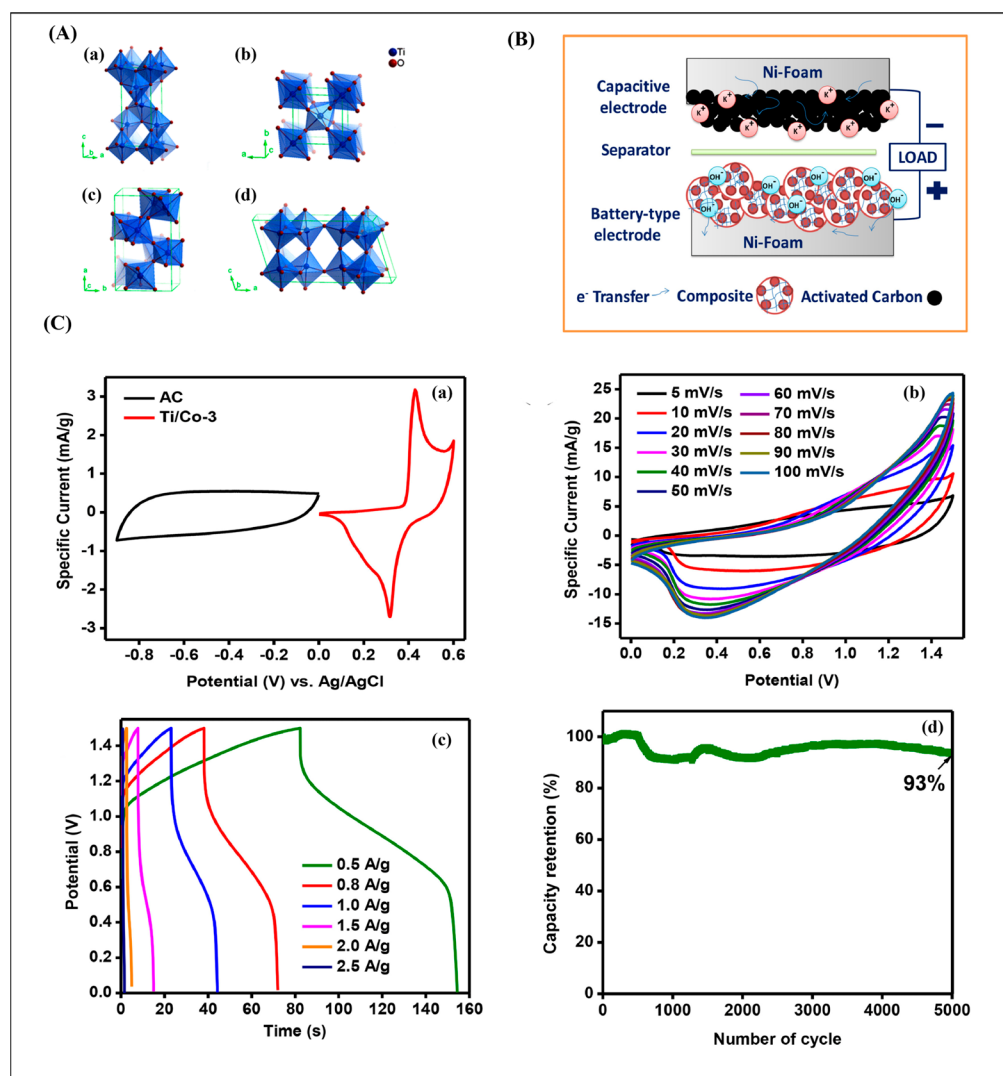


Figure 2. (A) Different crystalline phases of TiO₂: (a) anatase, (b) rutile, (c) brookite, and (d) TiO₂-B, reproduced with permission from ref. [77], American Chemical Society. (B) Schematic diagram of the HSC. (C) (a) Comparative CV of AC and TiO₂ aerogel/Co-MOF composite electrode, (b) CV of the HSC at different scan rates, and (c) GCD of the HSCs at various current rates, (d) Cycle stability of the AC and TiO₂ aerogel/Co-MOF electrodes, reproduced with permission from ref. [82], Elsevier.

Nonetheless, while TiO₂-MOF and other composite approaches successfully enhance conductivity, specific capacity, and mechanical stability, they introduce added complexity in synthetic steps and may face issues in large-scale reproducibility. MOFs, for example, can be expensive or sensitive to environmental conditions (e.g., humidity), potentially

limiting their viability for mass production. The integration of multiple components (TiO_2 aerogel + Co-MOF + carbon) must also ensure strong interfacial contact and consistent distribution across the electrode to avoid inhomogeneous regions that could degrade electrochemical performance.

6.1.2. $\text{Li}_4\text{Ti}_5\text{O}_{12}$

$\text{Li}_4\text{Ti}_5\text{O}_{12}$ (LTO) is a well-studied material as an intercalation type anode for Li-ion batteries due to its several advantages including low cost, long cycle life, and safety. LTO can accommodate three Li-ions per formula unit during cycling with two phase reactions and a negligible volume change of 0.2% (zero-strain) [83]. LTO is also a promising material for HSC but inherent issues like poor electronic conductivity ($2.7 \times 10^{-7} \text{ Scm}^{-1}$), poor ionic conductivity ($<10^{-12} \text{ cm}^2\text{s}^{-1}$), and poor rate capability inhibit the overall electrochemical performance of the HSC device [84,85]. Several methods are utilized to overcome these shortcomings and to enhance the performance of the HSC, such as nanosizing LTO to decrease the diffusion length, composite design with conducting materials like carbon, and doping with other elements like Al^{3+} , Cr^{3+} , or Mg^{2+} [86,87]. Naoi et al. coupled the nanosizing of LTO and composite design with carbon nanofibers (CNF) to attain high-rate capability and enhanced electrochemical performance [88]. They reported the successful synthesis of a high-rate-capable nanocrystalline LTO anode grafted on CNF (nc-LTO/CNF). The schematic of the formation process of nc-LTO/CNF is shown in Figure 3A, and the successful formation of nc-LTO/CNF is evident from the high-resolution transmission electron microscopy (HR-TEM) image of nc-LTO/CNF (as shown in Figure 3B). The enhanced rate capability of the nc-LTO/CNF-based electrochemical cell can be seen in Figure 3C. The HSC device comprising nc-LTO/CNF anode and AC cathode exhibits improved energy and power density compared to the conventional AC/AC symmetric supercapacitor. Also, the nc-LTO/CNF anode with a higher LTO weight percentage than CNF (70:30) shows better performance than the equal weight ratio between LTO and CNF (50:50) (as shown in Figure 3D). Kim and co-workers reported the synthesis of a composite of LTO and spherical holey graphene (HG) to enhance the electronic conductivity of LTO which arises from the high conductivity of graphene and high ionic transport arising from open pores in graphene sheets of HG [89]. The HSC device fabricated using spherical LTO/HG composite anode shows improved electrochemical performance compared to the HSC devices fabricated with LTO/RGO composite. The HSC device with LTO/HG composite anode delivered an energy density as high as 117.3 Wh.kg^{-1} , which arises from the synergistic effect of both components. Several other HSC devices with anode of modified LTO by carbon materials were also reported with enhanced electrochemical performances [90–92].

Nevertheless, despite the clear advantages of LTO-based anodes (particularly their near-zero strain and commendable safety features), several critical limitations need further scrutiny. First, while carbon or graphene-based modifications do effectively address the low conductivity, they increase the complexity and cost of synthesis—factors that can hinder large-scale commercial implementation. Second, the reduced volume change helps maintain mechanical integrity, but LTO's somewhat restricted operating voltage window and moderate theoretical capacity may limit the ultimate energy density achievable in HSC configurations. Third, doping with various cations (e.g., Al^{3+} and Mg^{2+}) can improve certain properties but may introduce trade-offs in terms of crystal stability or can demand precise processing conditions that complicate manufacturing. Finally, strict control over particle size and morphology is crucial for consistent, high-performance devices; batch-to-batch variability remains a challenge, particularly when scaling up nanosized LTO materials.

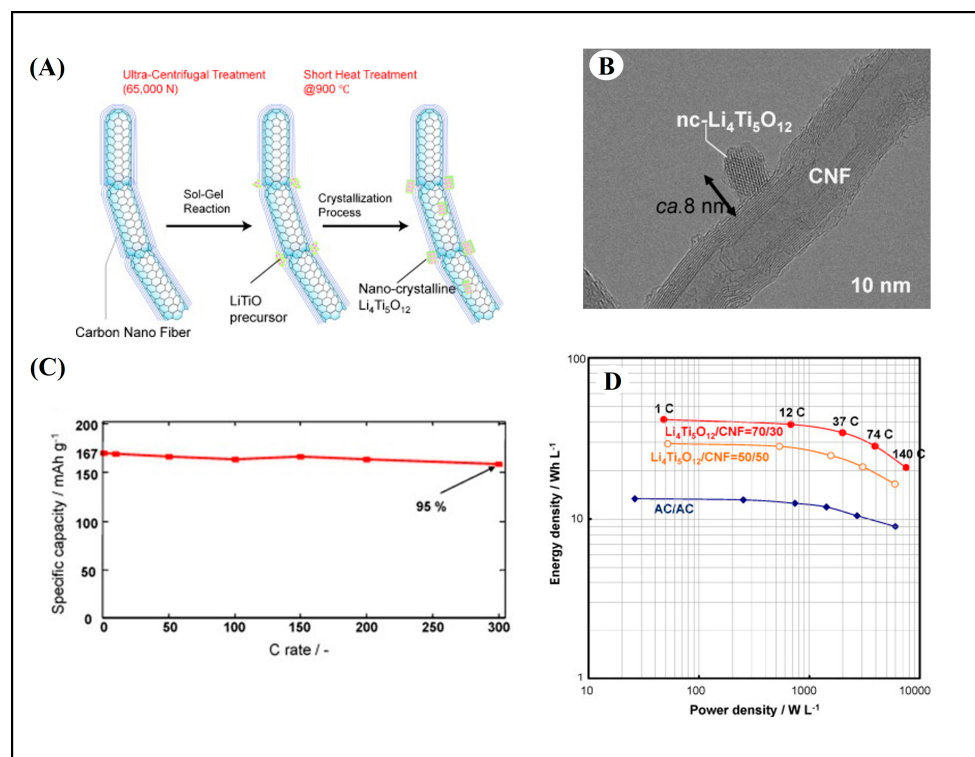


Figure 3. (A) schematic illustration for the two-step formation mechanism of the nc-LTO/CNF composite. (B) HR-TEM image of the nc-LTO/CNF composite. (C) rate capability of nc-LTO/CNF composite at different C-rates. (D) Ragone plots of LTO/CNF-based hybrid supercapacitors and AC/AC symmetric supercapacitor. Reproduced with permission from ref. [88], Elsevier.

6.2. Co-Based TMOs

Cobalt as an element plays a key role in battery cathode materials due to its good thermal stability and reversible redox capabilities [93]. In HSC, different Co-based materials such as spinel Co_3O_4 and other bi-metallic cobalt oxides are extensively explored as battery-type electrode materials [94].

6.2.1. Co_3O_4

In 2019, Devi et al. successfully synthesized a spinel Co_3O_4 using the sol–gel technique. They fabricated an HSC device using synthesized Co_3O_4 as a positive electrode, RGO as a negative electrode, and an aqueous-based electrolyte, with an enhanced energy density of 40 $\text{Wh}\cdot\text{kg}^{-1}$ at a power density of 742 $\text{W}\cdot\text{kg}^{-1}$ and Columbic efficiency of 98% [69], which signifies the applicability of Co_3O_4 as a battery-type electrode. Co_3O_4 with different morphologies were also reported to have enhanced electrochemical properties. For instance, Numan et al. reported an HSC with good electrochemical performance (specific capacity: 108 Cg^{-1} , energy density: 23.7 $\text{Wh}\cdot\text{kg}^{-1}$, power density: 307 $\text{W}\cdot\text{kg}^{-1}$) comprising a 2D porous Co_3O_4 nanoflakes (CONF) as positive electrode and an activated carbon as negative electrode in KOH electrolyte [95]. Park and co-workers reported a nano horn-like Co_3O_4 (NHC) using a solvothermal technique, a schematic of the synthesis process is shown in Figure 4A and the TEM image of the NHC is shown in Figure 4B. The authors also presented the influence of calcination temperature on the electrochemical performance of the NHC-containing HSC device [96]. The NHC calcined at 300 °C (NHC@300) shows the best electrochemical performance compared to other NHCs which are calcined at 350, 400, and 450 °C. CV curves of NHC@300 are comprised of well-defined redox peaks stemming from $\text{Co}^{2+}/\text{Co}^{3+}$ and $\text{Co}^{3+}/\text{Co}^{4+}$ redox couples (as shown in Figure 4C(a)). The high cathodic and anodic current values of NHC@300 in CV curve compared to NHC@350, 400, and

450 materials confirmed the enhanced electrochemical performance of NHC@300 (as shown in Figure 4C(b)). The enhanced electrochemical performance of NHC@300 stems from the enhanced diffusion kinetics of NHC@300 which is confirmed by the lowered resistance value in the Nyquist plot. The lowest equivalent series resistance (ESR) for NHC@300, which is evident from the intercepts in the high-frequency region of the X-axis and the steepness of the Warburg slope in the low-frequency region confirms the enhanced kinetics of NHC@300 compared to other NHCs (Figure 4C(c)). The plateaus in the galvanostatic charge–discharge (GCD) curves confirmed the battery-like behavior of synthesized NHCs as shown in Figure 4C(d). This plateau is more pronounced in NHC@300 than in other NHCs calcined at different temperatures as evident from Figure 4C(e). The enhanced specific capacitance of different of NHC@300 (2751 F g^{-1} at 1 A g^{-1}) compared to other NHCs confirmed the enhanced electrochemical performance of NHC@300 (as shown in Figure 4C(f)). The authors also evaluated the cycling stability of an HSC with NHC@300 as a positive electrode and AC as a negative electrode, they found 91.37% capacity retention even after 350,000 GCD cycles at 20 A g^{-1} of current density as can be seen in Figure 4D.

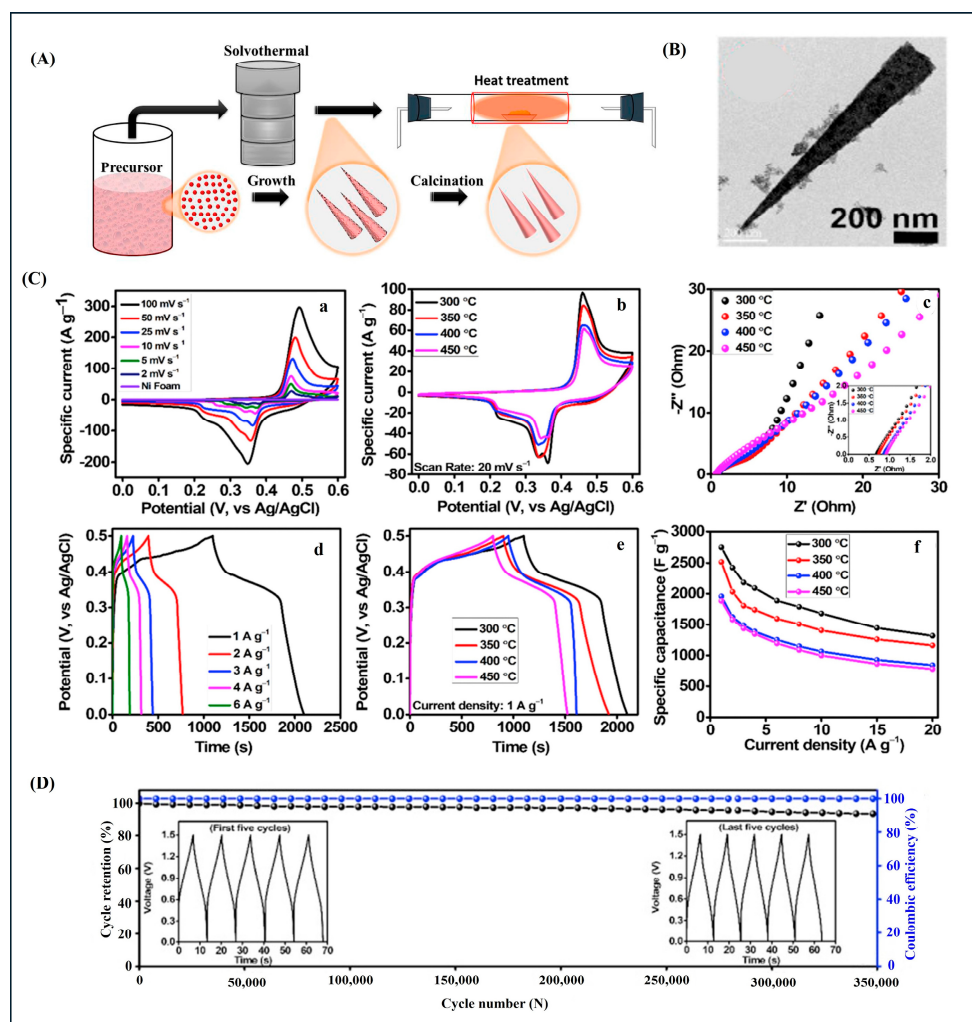


Figure 4. (A) schematic illustration of synthetic procedures and proposed formation mechanism of the Co_3O_4 nano horn. (B) TEM image of the synthesized nano horn. (C) (a) CV curve of NHC@300 at different scan rates, (b) CV curves of NHCs synthesized at different temperatures, (c) Nyquist plots of EIS for different NHCs, (d) GCD curves of NHC@300, (e) GCD curves of NHCs synthesized at different temperatures, and (f) specific capacitance of the NHCs at different current densities. (D) cycling stabilities and Coulombic efficiency of the NHC@300-based HSC. Reproduced with permission from ref. [96], Elsevier.

Apart from the morphologically different Co_3O_4 , Co_3O_4 coupled with different other materials were also reported and utilized in HSC applications. Vattikuti et al. reported the successful fabrication of an HSC device using carbon nitride/ Co_3O_4 material with improved electrochemical performance [97]. Arjunan et al. reported the synthesis of Co_3O_4 nanoparticles embedded in nitrogen-doped porous carbon spheres and utilized it in the fabrication of an HSC device. The fabricated HSC device shows an enhanced specific capacitance of $464 \text{ F}\cdot\text{g}^{-1}$ at a current density of $1 \text{ A}\cdot\text{g}^{-1}$ [98]. A composite of Co_3O_4 and carbon ($\text{Co}_3\text{O}_4/\text{C}$), derived from a cobalt-containing metal-organic framework (MOF), was reported by Kazemi and co-workers, they utilized this synthesized $\text{Co}_3\text{O}_4/\text{C}$ as a positive electrode to fabricate an HSC with improved electrochemical performance [99]. Different other Co_3O_4 -based materials were reported by researchers and their efficacy as a battery-type electrode in an HSC device was studied [100–102]

6.2.2. Co-Based Bi-Metallic Oxides

Bi-metallic oxides where other metals apart from Co are also present are extensively studied as an electrode material for HSC applications. For instance, Chen et al. reported the successful fabrication of an HSC device using bi-metallic manganese-cobalt oxide ($\text{MnCo}_2\text{O}_{4.5}$) as a cathode and AC as an anode with KOH electrolyte [103]. The $\text{MnCo}_2\text{O}_{4.5}$ -based HSC device shows enhanced electrochemical performance. The authors conducted electrochemical tests on the HSC device using different potential windows and different current densities. Figure 5A(a) shows the CV of the HSC device at a potential window ranging from 0 to 1.2 to 1.8 V at a scan rate of 10 mVs^{-1} . The potential window from 0–1.75 V was found suitable with negligible polarization phenomenon. Battery-like features can be observed in the GCD curves with low voltage drop (as shown in Figure 5A(b)). With the increase in operating potential, an increase in both specific capacity ($77.40 \text{ C}\cdot\text{g}^{-1}$ at 1.2 V to $126.29 \text{ C}\cdot\text{g}^{-1}$ at 1.75 V) and specific energy density ($15.02 \text{ Wh}\cdot\text{kg}^{-1}$ at 1.2 V to $33.36 \text{ Wh}\cdot\text{kg}^{-1}$ at 1.75 V) is observed as evident from Figure 5A(c,d). Battery-like redox behavior (peaks arise from Faradaic reactions) and capacitive behavior (distorted rectangular shape) are evident from the CV profiles of the HSC device at different scan rates as can be seen in Figure 5B(a). The appearance of the weak plateau region along with the distorted triangular shape in the GCD curve confirms the capacity contribution from both battery-like capacitive mechanisms arising from battery-type $\text{MnCo}_2\text{O}_{4.5}$ cathode and capacitive-type AC anode (as shown in Figure 5B(b)). The enhanced rate performance of the bimetallic cathode-based HSC device at different current densities is evident from Figure 5B(c). The $\text{MnCo}_2\text{O}_{4.5}$ -based HSC device showed enhanced cycling stability. No significant capacity decay was observed even after 5000 cycles (100.04% capacity retention), cycling at a current density as high as $6 \text{ A}\cdot\text{g}^{-1}$, which can be seen in Figure 5B(d). Nearly 100% Coulombic efficiency even after long-term cycling suggested good cycling stability of the $\text{MnCo}_2\text{O}_{4.5}$ -containing HSC device. $\text{MnCo}_2\text{O}_{4.5}$ with different morphologies were also reported and utilized as a battery-type electrode in HSC applications. For instance, urchin-like and micro flower-like $\text{MnCo}_2\text{O}_{4.5}$ bi-metallic oxides were synthesized by different research groups and used as battery-type electrodes in HSC devices with improved electrochemical performances [104,105]. Apart from $\text{MnCo}_2\text{O}_{4.5}$, other Mn, Co-based bi-metallic were also reported as a battery-type electrode for HSC [106–108].

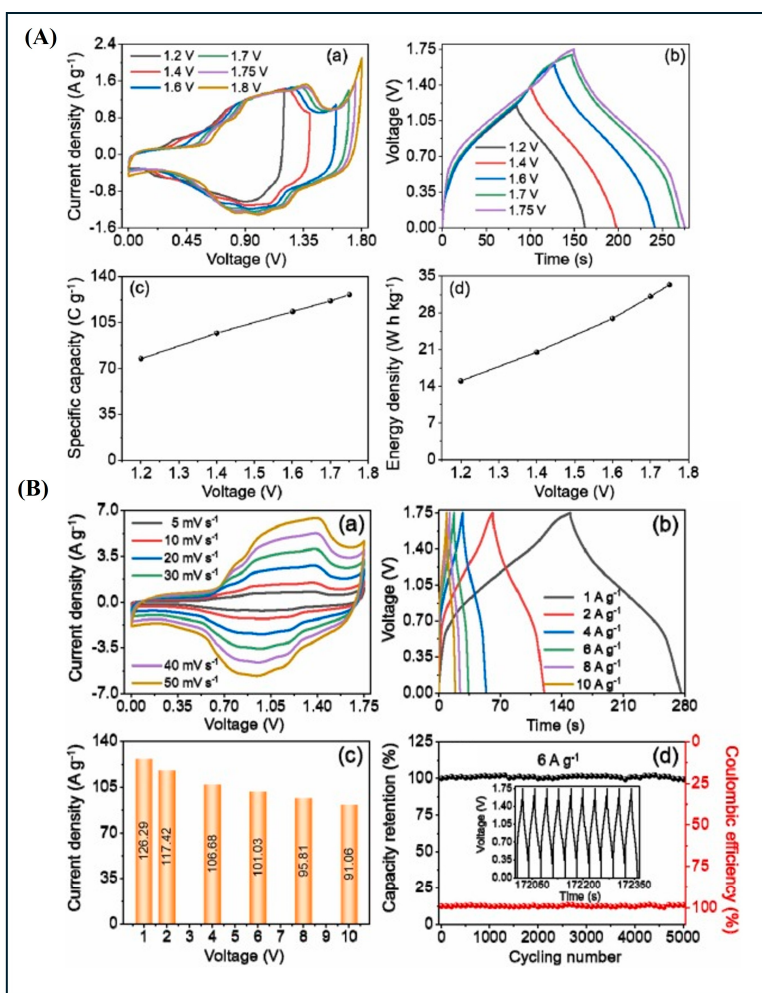


Figure 5. (A) (a) CV curves of $\text{MnCo}_2\text{O}_{4.5}$ -based HSC at different potential windows, (b) GCD curves of $\text{MnCo}_2\text{O}_{4.5}$ -based HSC at different potential windows, (c) The plot of specific capacitance as a function of voltage window for $\text{MnCo}_2\text{O}_{4.5}$ -based HSC, and (d) The plot of energy density as a function of voltage window for $\text{MnCo}_2\text{O}_{4.5}$ -based HSC. (B) (a) CV curves, (b) GCD curves, (c) rate performance, and (d) cycling performance and Coulombic efficiency of $\text{MnCo}_2\text{O}_{4.5}$ -based HSC. Reproduced with permission from ref. [103], Elsevier.

The efficacy of Co-based bi-metallic oxides with other metals towards battery-type electrodes in HSC devices were also explored extensively. Recently, Ahmad et al. reported an improvement in the electrochemical performance of an HSC using chromium–cobalt-based bi-metallic oxide (CrCo_2O_4) synthesized by hydrothermal method [109]. Both Cr and Co play synergistic role to enhance the electrochemical performance compared to their individual oxide counterparts (Co_3O_4 and Cr_2O_3). Figure 6A(a) shows the CV curves of bi-metallic CrCo_2O_4 , Cr_2O_3 , and Co_3O_4 , in the potential window of 0.0 to 0.55 V at a scan rate of 5 mVs^{-1} . Between these three oxides, the current response of CrCo_2O_4 is highest with the highest area under the CV curve which signifies the capacitance of the material. Figure 6A(b) shows the specific capacitance of the oxides at different current densities with 69.4% capacity retention for bimetallic CrCo_2O_4 , the highest compared to the other two individual metal oxides Cr_2O_3 (31.9%) and Co_3O_4 (60.7%). Enhanced diffusion-kinetics is one of the reasons behind the improved performance of the bi-metallic oxide. The bi-metallic CrCo_2O_4 possesses the lowest values for charge-transfer resistance (R_{ct}) and equivalent series resistance (R_s) with the value of $R_{ct} = 0.135 \Omega$, and $R_s = 0.64 \Omega$ compared to Cr_2O_3 (R_{ct} : 0.176Ω , R_s : 0.84Ω), and Co_3O_4 (R_{ct} : 0.156Ω , R_s : 0.87Ω) (as shown in Figure 6A(c)). The authors also conducted a long-term cycling test of the oxides

with a current density of $10 \text{ A}\cdot\text{g}^{-1}$. The CrCo_2O_4 shows the highest capacity retention of 98.74% even after 10,000 cycles, which is highest among the oxides with 97.34% retention for Co_3O_4 and 96.4% retention for Cr_2O_3 as evident from Figure 6B. To check the efficacy of the bi-metallic oxide as an electrode for an HSC device, authors fabricated an aqueous HSC using a CrCo_2O_4 -based positive electrode and AC as a negative electrode. Figure 6C shows the rate-performance of the HSC device at different current densities ranging from $1 \text{ A}\cdot\text{g}^{-1}$ to $20 \text{ A}\cdot\text{g}^{-1}$ with the number of cycles up to 400 cycles. Capacity retention as high as 72% of the initial capacity was obtained even after reaching a high current density of $20 \text{ A}\cdot\text{g}^{-1}$ with 98% Coulombic efficiency. The CrCo_2O_4 -based HSC device also shows a capacity retention of 97% after 10,000 cycles even at a current density of $10 \text{ A}\cdot\text{g}^{-1}$, which encompasses good cycling stability (as shown in Figure 6D). These enhanced performances of the CrCo_2O_4 -based device stem from the synergism between Cr and Co metals in the bi-metallic oxide—these cumulative effects are missing in individual oxides, and are therefore inferior to performance than their bi-metallic counterpart. Different other bi-metallic oxides such as CoWO_4 [110], FeCo_2O_4 [111], Cu_2CoO_3 [112], NiCo_2O_4 [113] and ZnCo_2O_4 [114] were also reported and utilized as battery-type electrode in an HSC device.

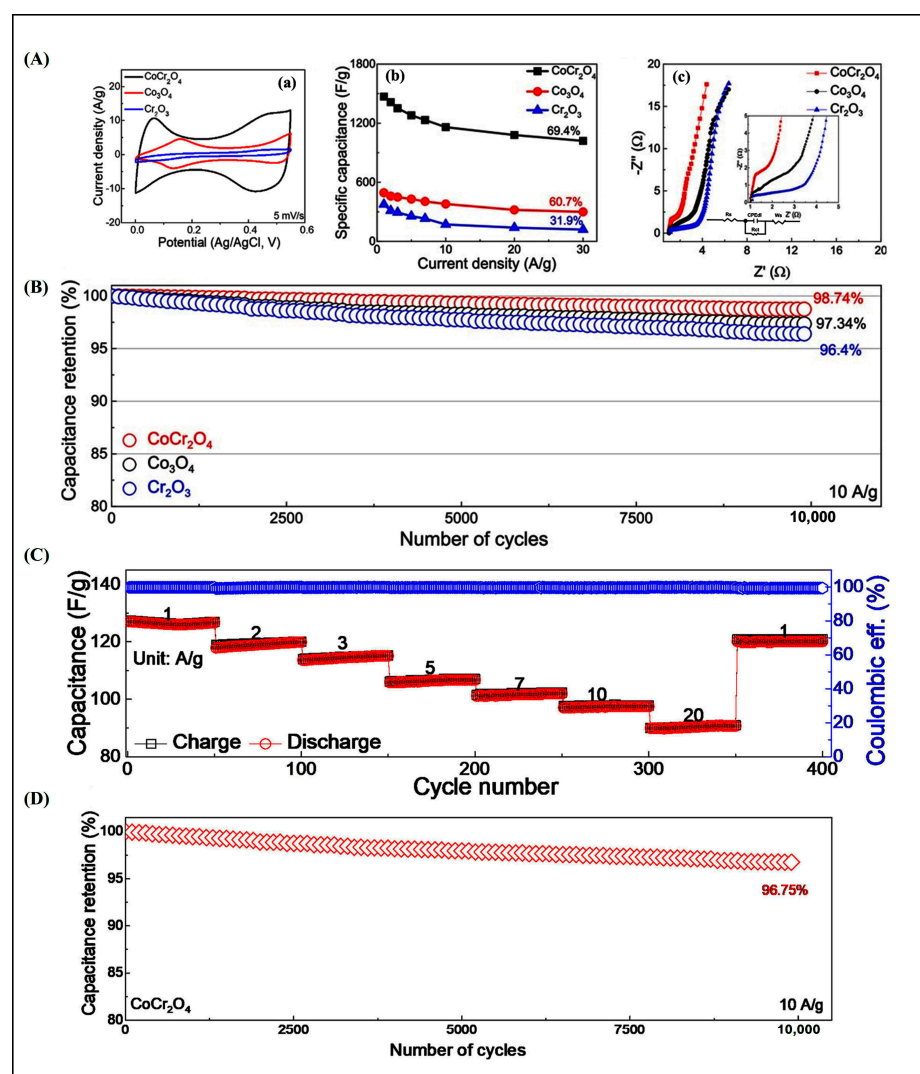


Figure 6. (A) (a) Comparative CV curves of CrCo_2O_4 , Co_3O_4 , and Cr_2O_3 , (b) specific capacitance at different current densities, and (c) EIS spectra of CrCo_2O_4 , Co_3O_4 , and Cr_2O_3 . (B) Cycling performance of CrCo_2O_4 , Co_3O_4 , and Cr_2O_3 . (C) Rate capability and Coulombic efficiency of CrCo_2O_4 -based HSC. (D) Long-term cycling stability of CrCo_2O_4 -based HSC at $10 \text{ A}\cdot\text{g}^{-1}$. Reproduced with permission from ref. [109], American Chemical Society.

Despite these promising outcomes, several challenges and limitations persist for Co-based TMOs. First, the intrinsic electronic conductivity of Co-based TMOs can remain suboptimal, necessitating complex morphologies or carbon integration to achieve high-rate capabilities. Second, engineering unique architectures (e.g., horn-like shapes, nanoflakes, or MOF-derived composites) often involves multiple synthesis steps that can be costly and difficult to reproduce consistently at large scales. Additionally, while Co-based TMO materials exhibit stable cycling in many lab-scale demonstrations, stability can still degrade under prolonged high-rate operations or in certain aqueous electrolytes. Finally, cobalt-based compounds raise concerns regarding cost fluctuations and potential environmental impacts related to cobalt extraction and processing. Future endeavors should thus focus on scalable, eco-friendly routes to form robust architecture and composites, as well as advanced characterization methods to unravel failure mechanisms in real time. Addressing these issues will be crucial for accelerating the commercial deployment of cobalt-based TMOs in HSCs with both high energy and power densities.

6.3. V-Based TMOs

Vanadium (V) is another attractive element used in energy storage applications like Li-ion, Na-ion batteries, multivalent batteries, and supercapacitors owing to its diverse oxidation states (from +2 to +5) [115–117].

V_2O_5

Among different vanadium-based compounds vanadium pentoxide (V_2O_5) stands out as a promising electrode material owing to its low cost, layered structure, high capacity, and straightforward synthesis process [115,118]. Although V_2O_5 is considered a promising material as a battery-type electrode, it is plagued with inherent issues like low electronic conductivity and low ionic diffusion kinetics. To counter these issues strategies like morphology tuning (acquiring high surface area or nanostructuring to reduce diffusion length), composite formation with conductive materials such as carbon materials, and pre-intercalation with hetero ions such as Li^+ to increase the interlayer spacing were explored [117,119,120]. Recently, Xu et al. reported the enhancement in ionic and electronic conductivity of V_2O_5 by incorporating Co^{2+} ions and polyaniline (PANI) between the layers of V_2O_5 (CoVO-PANI) and utilized it as a cathode material in Zn-ion hybrid supercapacitor (ZHSC) [121]. The fabricated ZHSC device with CoVO-PANI@CC as cathode, AC@CC as anode, and using Zn-based electrolyte shows enhanced electrochemical performance stemming from the synergistic effects of Co^{2+} and PANI. Figure 7A shows the fabrication process of CoVO-PANI. The higher capacitance of CoVO-PANI-based ZHSC is evident from the area of the CV curves compared to VO-PANI, CoVO, and VO-based ZHSC device, which also confirms the synergism between Co^{2+} and PANI in enhancing the performance of ZHSC (as shown in Figure 7B(a)). The enhanced specific capacitance of CoVO-PANI-based ZHSC is evident from GCD curves as can be seen in Figure 7B(b). The lowered charge-transfer resistance of CoVO-PANI-based ZHSC (R_{ct} : 0.45 Ω) shows the enhanced diffusion rate of Zn^{2+} ions. The ZHSC devices based on VO-PANI, CoVO, and VO exhibit much higher R_{ct} values signifying sluggish Zn^{2+} ion diffusion (as shown in Figure 7B(c)). The synergism of Co^{2+} and PANI is also evident from the enhanced areal capacitance and enhanced long-term cycling stability of CoVO-PANI-based ZHSC compared to its other counterparts. The CoVO-PANI-based ZHSC retained 81.37% of its initial capacitance even after 20,000 cycles at current density of 50 $\text{mA}\cdot\text{cm}^{-2}$ (as shown in Figure 7C(a) and 7C(b)). Owing to the enhanced performance of CoVO-PANI electrode, authors fabricated a flexible ZHSC device using PVA-Zn(OTF)₂ as gel electrolyte and utilized the fabricated flexible

ZHSC device to power a digital watch as can be seen in Figure 7D(a). The schematic structure of the flexible ZHSC device is shown in Figure 7D(b).

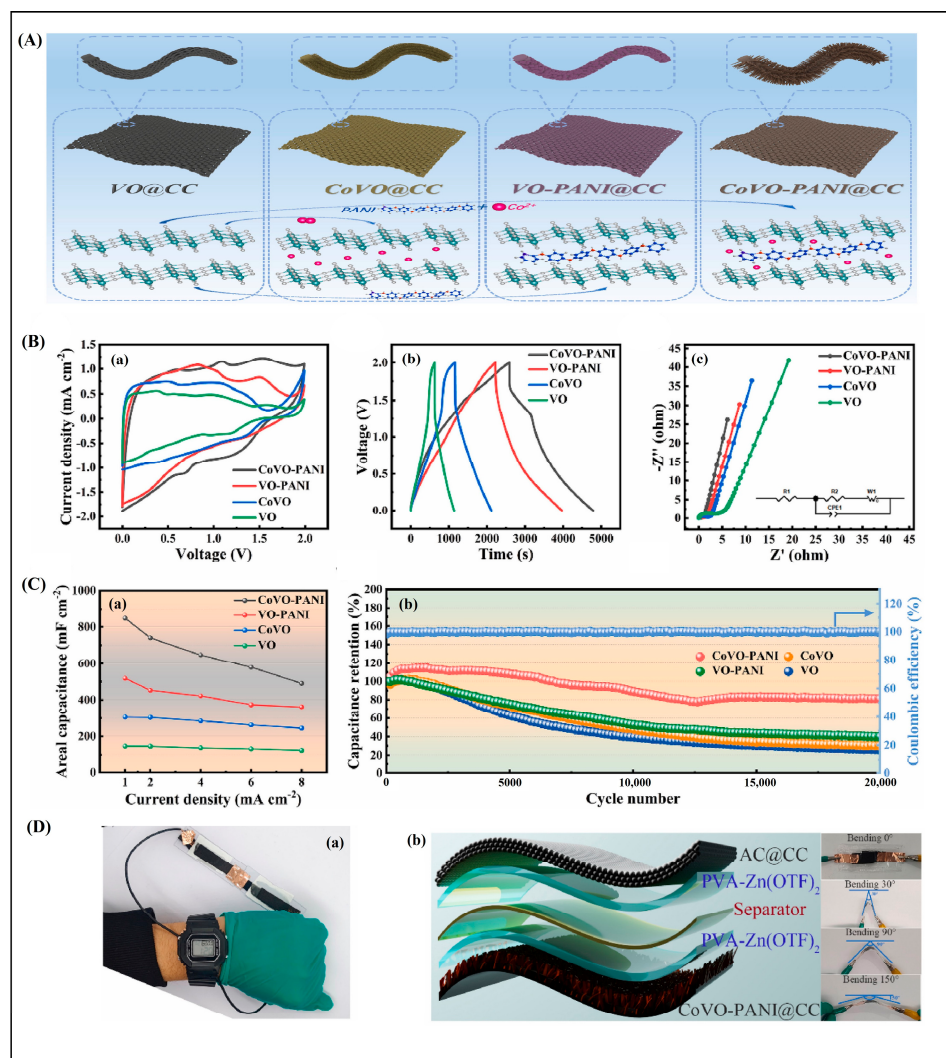


Figure 7. (A) preparation schematics of VO@CC, CoVO@CC, VO-PANI@CC, and CoVO-PANI@CC. (B) (a) CV curves of CoVO-PANI, VO-PANI, CoVO and VO at 1 mVs^{-1} , (b) GCD curves of CoVO-PANI, VO-PANI, CoVO and VO, and (c) EIS curves of CoVO-PANI, VO-PANI, CoVO and VO. (C) (a) areal capacitance curves of CoVO-PANI, VO-PANI, CoVO and VO at different current densities; (b) long-term cycling stability tests of CoVO-PANI, VO-PANI, CoVO and VO. (D) (a) Image of digital watch powered by flexible ZHSC devices; (b) schematic diagram of the fabrication flexible ZHSC device. Reproduced with permission from ref. [121].

Different other V_2O_5 , such as pre-lithiated V_2O_5 [122], hollow-structured V_2O_5 [123], V_2O_5 nanofibers [124], V_2O_5 /graphene oxide nanocomposites [125] were also reported as an electrode material for HSC applications, demonstrating significant improvements in performance compared to their unmodified counterparts. These structural and compositional modifications address the inherent limitations of pristine V_2O_5 , such as low electrical conductivity, poor cycling stability, and limited rate capability. Pre-lithiated V_2O_5 , for instance, benefits from a pre-intercalation strategy that introduces lithium ions into the V_2O_5 lattice, resulting in enhanced electrical conductivity and reduced lattice strain during the charge/discharge cycles. This modification not only stabilizes the crystal structure but also boosts the overall capacity and cycling life of the electrode. Hollow-structured V_2O_5 takes advantage of its unique architecture, which provides a high surface area, reduced ion diffusion pathways, and improved electrolyte penetration. These features significantly enhance

the redox reaction kinetics and increase the electrode's ability to store and deliver charge efficiently. V_2O_5 nanofibers, synthesized through electrospinning and other advanced fabrication methods, offer a one-dimensional structure with excellent electron transport properties and a high aspect ratio. The interconnected network of nanofibers facilitates rapid ion and electron transfer, making them particularly suitable for high power applications. V_2O_5 /graphene oxide nanocomposites represent another promising approach, where the synergistic combination of V_2O_5 's redox activity and graphene oxide's high conductivity and mechanical stability results in superior electrochemical performance. The graphene oxide not only enhances the electrical conductivity of the composite but also prevents the agglomeration of V_2O_5 particles, ensuring a more stable cycling performance.

To provide a clear comparison of the electrochemical performance of transition metal oxide (TMO) battery-type electrodes in hybrid supercapacitors, a tabulated summary of specific power and energy densities is presented in Table 1. This comprehensive overview will help readers quickly assess the relative merits of various TMO-based systems, including cycling performance, energy density and power density.

Table 1. The performance matrices of different HSCs based on TMOs.

TMO-Based HSC	Synthesis	Energy Density (Whkg^{-1})	Power Density (Wkg^{-1})	Cycling Stability	Reference
$\text{Co}_3\text{O}_4@\text{Mn-Ni(OH)}_2/\text{CC}$	Hydrothermal	65.5	800	93.0%, 10,000 cycles	[126]
$\text{Co}_3\text{O}_4/\text{Ni}/\text{N@g-C}_3\text{N}_4$	Hydrothermal	22.26	4000	82.4% 5000 cycles,	[127]
$\text{Co}_3\text{O}_4 \text{ MBs}/\text{AC}$	Hydrothermal	38.5	962	126.4%, 5000 cycles	[128]
$\text{Co}_3\text{O}_4//\text{rGO}$	Sol-gel	40	742	-	[69]
$\text{MnCo}_2\text{O}_4//\text{AC}$	Aqueous chemical synthesis	36	4274	91.1%, 5000 cycles	[129]
$\text{CoFe}_2\text{O}_4/\text{Cr}_2\text{CTx}/\text{AC}$	Hydrothermal	125	15,264.4	99%, 2500 cycles	[130]
$\text{MWCNT/LiCo}_2\text{O}_4//\text{AC}$	Co-precipitation	54.84	775	94%, 5000 cycles	[131]
$\text{Nio@Co}_3\text{O}_4/\text{C}/\text{AC}$	Precipitation method	32.6	750	87.1%, 5000 cycles	[132]
$\text{CoFe}_2\text{O}_4//\text{NPC}$	Reflux condensation	56.2	1091.5	97.91%, 5000 cycles	[133]
$\text{Fe}_3\text{O}_4 \text{ NPs}$	Solvothermal	152.06	1822	89.71%, 5000 cycles	[134]
$\text{Ni}_x\text{Fe}_y\text{O}_2@\text{rGO}/\text{AC}$	Microwave synthesis	43	2500	86%, 1000 cycles	[135]
$\text{Li}_3\text{VO}_4//\text{AC}$	Hydrothermal	136.4	532	87%, 1500 cycles	[136]
$\text{Li}_3\text{VO}_4@\text{C}/\text{AC}$	Micro-emulsion-based method	190	18,500	-	[137]
$3\text{DG}/\text{Ni}_{x}\text{Co}_{1-x}\text{O}/3\text{DG}$	Spontaneous assembly process	27.2	14,500	86%, 10,000 cycles	[138]
$\text{NiCo-P/Ni}_3\text{V}_2\text{O}_8//\text{AC}$	Hydrothermal	65	750	84.21%, 10,000 cycles	[139]
$\text{ZnCo}_2\text{O}_4 \text{ NSs}/\text{AC}$	Hydrothermal	43.88	1077.45	~100%, 8000 cycles	[140]
$\text{CrCo}_2\text{O}_4/\text{AC/PPY}/\text{MnO}_2/\text{AC}$	Hydrothermal	97.77	1600	76.75%, 10,000 cycles	[141]
$\text{Cu-Mn-Zn Oxide}/\text{AC}$	Hydrothermal	44.26	9432.69	86.65%, 3000 cycles	[142]
$\text{ZnCr}_2\text{O}_4@\text{CC}/\text{AC}$	Hydrothermal	26.2	800.6	96.43%, 10,000 cycles	[143]

7. Conclusions and Future Direction

Hybrid supercapacitors (HSCs) represent a transformative advancement in energy storage technologies, effectively bridging the gap between batteries and supercapacitors by combining high energy density with excellent power density. This review has highlighted the critical role of transition metal oxides (TMOs) as battery-type electrodes, underscoring their capacity for Faradaic redox reactions that enable robust charge storage while retaining formidable power performance. Across the broad spectrum of synthesis techniques, spanning hydro/solvothermal processes, electrospinning, electrodeposition, and sol-gel methods, researchers have demonstrated how careful control of TMO structures

and morphologies can mitigate key limitations such as low electrical conductivity and restricted ionic diffusion. The spotlight on Ti-, Co-, and V-based TMOs, in particular, illustrates how strategies like nanostructuring, composite integration, and doping can boost electrochemical outputs.

Nonetheless, certain challenges must be tackled for TMO-based HSCs to achieve commercial readiness such as (i) cycling stability: while striving for higher energy density, TMOs undergo substantial volumetric changes during ion insertion/extraction, which can lead to microcracks and structural deformation. This underscores the delicate balance between boosting capacity and preserving electrode integrity over extended cycles. (ii) Scalability: many of the advanced nanostructuring and composite methods that deliver excellent lab-scale performance can be difficult or costly to implement at industrial scales, necessitating more streamlined, cost-effective manufacturing processes. (iii) Cost-effectiveness: high-performance materials and specialized synthesis conditions can drive up production expenses. Achieving a favorable balance of performance and affordability is paramount for real-world adoption.

Looking ahead, the future outlook for TMO-based HSCs hinges on integrating innovative research avenues and practical engineering solutions. Emerging strategies for developing advanced TMO electrodes concentrate on simultaneously boosting electrochemical performance and maintaining structural resilience, including (i) defect engineering: creating and tailoring oxygen vacancies or interstitials to regulate ion transport and accommodating volume expansion [144,145]. (ii) Hierarchical nanostructures: designing multi-level architectures, such as core–shell or hollow structures, that offer larger reactive surface areas while tolerating mechanical strain more effectively [146]. (iii) Functional coatings and protective layers: using thin coatings (e.g., polymeric, metallic, or carbonaceous layers) to stabilize electrode surfaces, mitigate unwanted side reactions, and reduce structural deterioration [147]. (iv) Hybrid composites with 2D materials: incorporating emerging two-dimensional materials (like graphene derivatives or MXenes) to reinforce conductivity, boost mechanical integrity, and provide additional ion diffusion channels [146]. (v) In situ/operando characterization tools: developing advanced analytical techniques to monitor structural evolution and reaction kinetics in real time, enabling more targeted material and device optimization [147].

Beyond these emerging strategies, there are several additional avenues with potential to advance TMO-based HSCs further:

1. Advanced Material Design

Innovations in defect chemistry, nanostructured morphologies, and composite interfaces can significantly improve both energy/power densities and mechanical resilience.

2. Sustainable Synthesis Methods

Green chemistry principles, eco-friendly solvents, and the recycling or reuse of precursors will be essential for minimizing environmental impact and reducing costs associated with large-scale production.

3. Flexible and Wearable HSCs

Architectures capable of withstanding mechanical stress under bending or stretching broaden the scope of HSC usage in consumer electronics and wearable technologies.

4. Machine Learning and Computational Modeling

High-throughput simulations and predictive algorithms can accelerate the discovery of new TMO compositions, dopants, and architectures, helping to efficiently pinpoint the most promising optimization pathways.

By focusing on these interconnected goals, enhancing cycling stability, refining scalability, and ensuring economic viability, TMO-based HSCs can continue to evolve as a cornerstone of next-generation energy storage. As researchers deepen their mechanistic insights and leverage computational tools, we can expect further breakthroughs that balance high energy density, structural robustness, and environmental sustainability, ultimately driving the widespread adoption of HSCs in a variety of commercial and industrial applications. All the challenges of HSCs and future directions for TMO-based HSCs are summarized schematically in Figure 8.

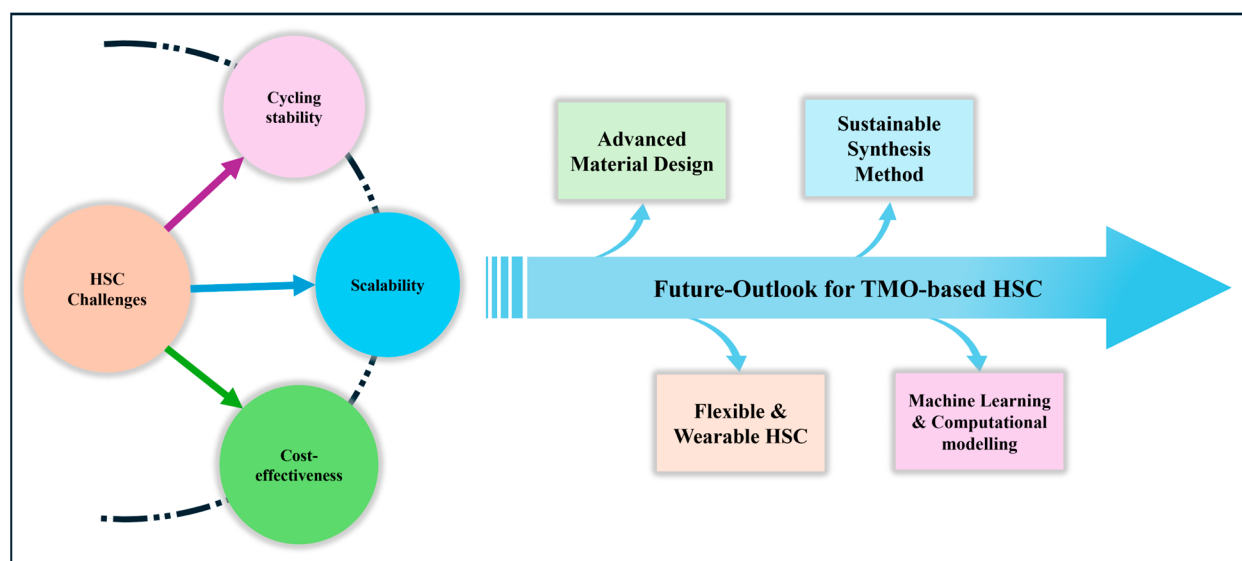


Figure 8. Schematic representation of challenges faced by HSCs and future directions for TMO-based HSCs.

In conclusion, HSCs hold immense potential to revolutionize energy storage by combining the best attributes of batteries and supercapacitors. Continued interdisciplinary research encompassing materials science, electrochemistry, and device engineering will be essential to overcome existing challenges and unlock the full potential of HSCs for a sustainable and energy-efficient future.

Author Contributions: Conceptualization, B.R., M.I., M.M.R.K. and G.A.K.M.R.B.; validation: M.S.A., M.M.R.K. and H.-Y.K.; data curation, G.A.K.M.R.B. and H.-Y.K.; funding acquisition, K.-W.N.; resources, K.-W.N.; supervision, M.I., and K.-W.N.; writing—original draft, B.R.; writing—review and editing, M.I., M.S.A. and K.-W.N. All authors have read and agreed to the published version of the manuscript.

Funding: This work was supported by the Ministry of Trade, Industry & Energy (MOTIE) of the Republic of Korea (Grant No. RS-2022-00155717 and 20224000000020).

Data Availability Statement: Not applicable.

Conflicts of Interest: The authors declare no conflicts of interest.

References

1. Liu, H.; Liu, X.; Wang, S.; Liu, H.K.; Li, L. Transition Metal Based Battery-Type Electrodes in Hybrid Supercapacitors: A Review. *Energy Storage Mater.* **2020**, *28*, 122–145. [[CrossRef](#)]
2. Simon, P.; Gogotsi, Y.; Dunn, B. Where Do Batteries End and Supercapacitors Begin? *Science* **2014**, *343*, 1208–1210. [[CrossRef](#)] [[PubMed](#)]
3. Winter, M.; Brodd, R.J. What Are Batteries, Fuel Cells, and Supercapacitors? *Chem. Rev.* **2004**, *104*, 4245–4269. [[CrossRef](#)] [[PubMed](#)]
4. Goodenough, J.B. How We Made the Li-Ion Rechargeable Battery. *Nat. Electron.* **2018**, *1*, 204. [[CrossRef](#)]

5. Ponrouch, A.; Bitenc, J.; Dominko, R.; Lindahl, N.; Johansson, P.; Palacin, M.R. Multivalent Rechargeable Batteries. *Energy Storage Mater.* **2019**, *20*, 253–262. [[CrossRef](#)]
6. Palacín, M.R. Recent Advances in Rechargeable Battery Materials: A Chemist’s Perspective. *Chem. Soc. Rev.* **2009**, *38*, 2565–2575. [[CrossRef](#)]
7. Gicha, B.B.; Tufa, L.T.; Nwaji, N.; Hu, X.; Lee, J. Advances in All-Solid-State Lithium–Sulfur Batteries for Commercialization. *Nano-Micro Lett.* **2024**, *16*, 172. [[CrossRef](#)]
8. Ragone, D.V.; Ragone, D.V. *Review of Battery Systems for Electrically Powered Vehicles Review of Battery Systems for Electrically Powered Vehicles*; SAE: Warrendale, PA, USA, 2018.
9. Beyers, I.; Bensmann, A.; Hanke-Rauschenbach, R. Ragone Plots Revisited: A Review of Methodology and Application across Energy Storage Technologies. *J. Energy Storage* **2023**, *73*, 109097. [[CrossRef](#)]
10. Christen, T.; Carlen, M.W. Theory of Ragone Plots. *J. Power Sources* **2000**, *91*, 210–216. [[CrossRef](#)]
11. Wang, C.Y.; Liu, T.; Yang, X.G.; Ge, S.; Stanley, N.V.; Rountree, E.S.; Leng, Y.; McCarthy, B.D. Fast Charging of Energy-Dense Lithium-Ion Batteries. *Nature* **2022**, *611*, 485–490. [[CrossRef](#)]
12. Kim, U.H.; Lee, S.B.; Park, N.Y.; Kim, S.J.; Yoon, C.S.; Sun, Y.K. High-Energy-Density Li-Ion Battery Reaching Full Charge in 12 Min. *ACS Energy Lett.* **2022**, *7*, 3880–3888. [[CrossRef](#)]
13. Frith, J.T.; Lacey, M.J.; Ulissi, U. A Non-Academic Perspective on the Future of Lithium-Based Batteries. *Nat. Commun.* **2023**, *14*, 420. [[CrossRef](#)] [[PubMed](#)]
14. Satpathy, S.; Das, S.; Bhattacharyya, B.K. How and Where to Use Super-Capacitors Effectively, an Integration of Review of Past and New Characterization Works on Super-Capacitors. *J. Energy Storage* **2020**, *27*, 101044. [[CrossRef](#)]
15. Kumar, Y.A.; Roy, N.; Ramachandran, T.; Hussien, M.; Moniruzzaman, M.; Joo, S.W. Shaping the Future of Energy: The Rise of Supercapacitors Progress in the Last Five Years. *J. Energy Storage* **2024**, *98*, 113040. [[CrossRef](#)]
16. Zhang, M.; Du, H.; Wei, Z.; Zhang, X.; Wang, R. Ultrafast Microwave Synthesis of Nickel-Cobalt Sulfide/Graphene Hybrid Electrodes for High-Performance Asymmetrical Supercapacitors. *ACS Appl. Energy Mater.* **2021**, *4*, 8262–8274. [[CrossRef](#)]
17. Zhang, M.; Nautiyal, A.; Du, H.; Wei, Z.; Zhang, X.; Wang, R. Electropolymerization of Polyaniline as High-Performance Binder Free Electrodes for Flexible Supercapacitor. *Electrochim. Acta* **2021**, *376*, 138037. [[CrossRef](#)]
18. Dubal, D.P.; Ayyad, O.; Ruiz, V.; Gómez-Romero, P. Hybrid Energy Storage: The Merging of Battery and Supercapacitor Chemistries. *Chem. Soc. Rev.* **2015**, *44*, 1777–1790. [[CrossRef](#)]
19. Ding, J.; Hu, W.; Paek, E.; Mitlin, D. Review of Hybrid Ion Capacitors: From Aqueous to Lithium to Sodium. *Chem. Rev.* **2018**, *118*, 6457–6498. [[CrossRef](#)]
20. Zuo, W.; Li, R.; Zhou, C.; Li, Y.; Xia, J.; Liu, J. Battery-Supercapacitor Hybrid Devices: Recent Progress and Future Prospects. *Adv. Sci.* **2017**, *4*, 1600539. [[CrossRef](#)]
21. Cakici, M.; Reddy, K.R.; Alonso-Marroquin, F. Advanced Electrochemical Energy Storage Supercapacitors Based on the Flexible Carbon Fiber Fabric-Coated with Uniform Coral-like MnO₂ Structured Electrodes. *Chem. Eng. J.* **2017**, *309*, 151–158. [[CrossRef](#)]
22. Pramitha, A.; Raviprakash, Y. Recent Developments and Viable Approaches for High-Performance Supercapacitors Using Transition Metal-Based Electrode Materials. *J. Energy Storage* **2022**, *49*, 104120. [[CrossRef](#)]
23. Yuan, S.; Duan, X.; Liu, J.; Ye, Y.; Lv, F.; Liu, T.; Wang, Q.; Zhang, X. Recent Progress on Transition Metal Oxides as Advanced Materials for Energy Conversion and Storage. *Energy Storage Mater.* **2021**, *42*, 317–369. [[CrossRef](#)]
24. Chen, H.; Du, X.; Liu, X.; Wu, R.; Li, Y.; Xu, C. Facile growth of nickel foam-supported MnCo₂O₄. 5 porous nanowires as binder-free electrodes for high-performance hybrid supercapacitors. *J. Energy Storage* **2022**, *50*, 104297. [[CrossRef](#)]
25. Subhadarshini, S.; Peyada, N.K.; Goswami, D.K.; Das, N.C. Review of Battery-Type Transition Metal (Cu, Co, and Ni) Oxide Based Electrodes: From Fundamental Science to Fabrication of a Hybrid Supercapacitor Device. *Energy Fuels* **2024**, *38*, 11455–11493. [[CrossRef](#)]
26. Stepanov, A.B.; Varakin, I.N.; Menukhov, V.V. Double-Layer Capacitor. U.S. Patent 5,986,876, 16 November 1999.
27. Aida, T.; Yamada, K.; Morita, M. An Advanced Hybrid Electrochemical Capacitor That Uses a Wide Potential Range at the Positive Electrode. *Electrochim. Solid-State Lett.* **2006**, *9*, 534–536. [[CrossRef](#)]
28. Naoi, K. “Nanohybrid Capacitor”: The next Generation Electrochemical Capacitors. *Fuel Cells* **2010**, *10*, 825–833. [[CrossRef](#)]
29. Naoi, K.; Simon, P. New Materials and New Configurations for Advanced Electrochemical Capacitors. *Electrochim. Soc. Interface* **2008**, *17*, 34–37. [[CrossRef](#)]
30. Yoo, H.D.; Han, S.D.; Bayliss, R.D.; Gewirth, A.A.; Genorio, B.; Rajput, N.N.; Persson, K.A.; Burrell, A.K.; Cabana, J. “rocking-Chair”-Type Metal Hybrid Supercapacitors. *ACS Appl. Mater. Interfaces* **2016**, *8*, 30853–30862. [[CrossRef](#)]
31. Nitta, N.; Wu, F.; Lee, J.T.; Yushin, G. Li-Ion Battery Materials: Present and Future. *Mater. Today* **2015**, *18*, 252–264. [[CrossRef](#)]
32. Schmidt-Rohr, K. How Batteries Store and Release Energy: Explaining Basic Electrochemistry. *J. Chem. Educ.* **2018**, *95*, 1801–1810. [[CrossRef](#)]
33. Salanne, M.; Rotenberg, B.; Naoi, K.; Kaneko, K.; Taberna, P.L.; Grey, C.P.; Dunn, B.; Simon, P. Efficient Storage Mechanisms for Building Better Supercapacitors. *Nat. Energy* **2016**, *1*, 16070. [[CrossRef](#)]

34. Miller, J.R.; Simon, P. Materials Science: Electrochemical Capacitors for Energy Management. *Science* **2008**, *321*, 651–652. [CrossRef] [PubMed]
35. Huang, J.; Xie, Y.; You, Y.; Yuan, J.; Xu, Q.; Xie, H.; Chen, Y. Rational Design of Electrode Materials for Advanced Supercapacitors: From Lab Research to Commercialization. *Adv. Funct. Mater.* **2023**, *33*, 2213095. [CrossRef]
36. Gogotsi, Y.; Simon, P. True Performance Metrics in Electrochemical Energy Storage. *Science* **2011**, *334*, 917–918. [CrossRef]
37. Lindström, H.; Södergren, S.; Solbrand, A.; Rensmo, H.; Hjelm, J.; Hagfeldt, A.; Lindquist, S.E. Li⁺ Ion Insertion in TiO₂ (Anatase). 1. Chronoamperometry on CVD Films and Nanoporous Films. *J. Phys. Chem. B* **1997**, *101*, 7710–7716. [CrossRef]
38. Bard, A.J. *Fundamentals and Applications Plasmonics: Fundamentals and Applications*; Springer: Berlin/Heidelberg, Germany, 2004; Volume 677.
39. Dong, Y.; Li, D.; Gao, C.; Liu, Y.; Zhang, J. A Self-Assembled 3D Urchin-like Ti_{0.8}Sn_{0.2}O₂-RGO Hybrid Nanostructure as an Anode Material for High-Rate and Long Cycle Life Li-Ion Batteries. *J. Mater. Chem. A* **2017**, *5*, 8087–8094. [CrossRef]
40. Noori, A.; El-Kady, M.F.; Rahmanifar, M.S.; Kaner, R.B.; Mousavi, M.F. Towards Establishing Standard Performance Metrics for Batteries, Supercapacitors and Beyond. *Chem. Soc. Rev.* **2019**, *48*, 1272–1341. [CrossRef]
41. Yang, P.; Ding, Y.; Lin, Z.; Chen, Z.; Li, Y.; Qiang, P.; Ebrahimi, M.; Mai, W.; Ping Wong, C.; Lin Wang, Z. Low-Cost High-Performance Solid-State Asymmetric Supercapacitors Based on MnO₂ Nanowires and Fe₂O₃ Nanotubes. *Nano Lett.* **2014**, *14*, 731–736. [CrossRef]
42. Chen, H.; Du, X.; Wu, R.; Wang, Y.; Sun, J.; Zhang, Y.; Xu, C. Facile Hydrothermal Synthesis of Porous MgCo₂O₄ nanoflakes as an Electrode Material for High-Performance Asymmetric Supercapacitors. *Nanoscale Adv.* **2020**, *2*, 3263–3275. [CrossRef]
43. Mohamed, S.G.; Chen, C.J.; Chen, C.K.; Hu, S.F.; Liu, R.S. High-Performance Lithium-Ion Battery and Symmetric Supercapacitors Based on FeCo₂O₄ Nanoflakes Electrodes. *ACS Appl. Mater. Interfaces* **2014**, *6*, 22701–22708. [CrossRef]
44. Lee, J.W.; Hall, A.S.; Kim, J.D.; Mallouk, T.E. A Facile and Template-Free Hydrothermal Synthesis of Mn₃O₄ Nanorods on Graphene Sheets for Supercapacitor Electrodes with Long Cycle Stability. *Chem. Mater.* **2012**, *24*, 1158–1164. [CrossRef]
45. Chen, H.; Du, X.; Sun, J.; Wang, Y.; Zhang, Y.; Xu, C. Solvothermal Synthesis of Novel Pod-like MnCo₂O_{4.5} Microstructures as High-Performance Electrode Materials for Supercapacitors. *Int. J. Hydrog. Energy* **2020**, *45*, 3016–3027. [CrossRef]
46. Ankinapalli, O.R.; Krishna, B.N.V.; Ayyaluri, R.R.; Yu, J.S. ZnMoO₄/MoO₃ Composite Materials via Facile One-Step Hydrothermal Route for Efficient Hybrid Supercapacitors. *J. Energy Storage* **2024**, *85*, 111043. [CrossRef]
47. Sun, L.; Deng, Q.; Li, Y.; Deng, L.; Wang, Y.; Ren, X.; Zhang, P. Solvothermal Synthesis of Ternary Cu₂O-CuO-RGO Composites as Anode Materials for High Performance Lithium-Ion Batteries. *Electrochim. Acta* **2016**, *222*, 1650–1659. [CrossRef]
48. Kaneti, Y.V.; Zakaria, Q.M.D.; Zhang, Z.; Chen, C.; Yue, J.; Liu, M.; Jiang, X.; Yu, A. Solvothermal Synthesis of ZnO-Decorated α-Fe₂O₃ Nanorods with Highly Enhanced Gas-Sensing Performance toward n-Butanol. *J. Mater. Chem. A* **2014**, *2*, 13283–13292. [CrossRef]
49. Pullanchiyodan, A.; Joy, R.; Sreeram, P.; Raphael, L.R.; Das, A.; Balakrishnan, N.T.M.; Ahn, J.H.; Vlad, A.; Sreejith, S.; Raghavan, P. Recent Advances in Electrospun Fibers Based on Transition Metal Oxides for Supercapacitor Applications: A Review. *Energy Adv.* **2023**, *2*, 922–947. [CrossRef]
50. Kenawy, E.R.; Moharram, Y.I.; Abouharga, F.S.; Elfiky, M. Electrospun Network Based on Polyacrylonitrile-Polyphenyl/Titanium Oxide Nanofibers for High-Performance Supercapacitor Device. *Sci. Rep.* **2024**, *14*, 6683. [CrossRef]
51. Cao, Y.; Lin, B.; Sun, Y.; Yang, H.; Zhang, X. Sr-Doped Lanthanum Nickelate Nanofibers for High Energy Density Supercapacitors. *Electrochim. Acta* **2015**, *174*, 41–50. [CrossRef]
52. Lu, Y.; Liu, Y.; Mo, J.; Deng, B.; Wang, J.; Zhu, Y.; Xiao, X.; Xu, G. Construction of Hierarchical Structure of Co₃O₄ Electrode Based on Electrospinning Technique for Supercapacitor. *J. Alloys Compd.* **2021**, *853*, 157271. [CrossRef]
53. Ghaziani, M.M.; Mazloom, J.; Ghodsi, F.E. Electrospun MgCo₂O₄ Nanofibers as an Efficient Electrode Material for Pseudocapacitor Applications: Effect of Calcination Temperature on Electrochemical Performance. *J. Phys. Chem. Solids* **2021**, *152*, 109981. [CrossRef]
54. Yang, S.; Ai, J.; Han, Z.; Zhang, L.; Zhao, D.; Wang, J.; Yang, C.; Cao, B. Electrospun ZnFe₂O₄/Carbon Nanofibers as High-Rate Supercapacitor Electrodes. *J. Power Sources* **2020**, *469*, 228416. [CrossRef]
55. Bhagwan, J.; Sahoo, A.; Yadav, K.L.; Sharma, Y. Porous, One Dimensional and High Aspect Ratio Mn₃O₄ Nanofibers: Fabrication and Optimization for Enhanced Supercapacitive Properties. *Electrochim. Acta* **2015**, *174*, 992–1001. [CrossRef]
56. Liang, J.; Bu, L.T.; Cao, W.G.; Chen, T.; Cao, Y.C. Facile Fabrication of Coaxial-Cable like Mn₂O₃ Nanofiber by Electrospinning: Application as Electrode Material for Supercapacitor. *J. Taiwan Inst. Chem. Eng.* **2016**, *65*, 584–590. [CrossRef]
57. Xu, L.; Zhang, L.; Cheng, B.; Yu, J. Rationally Designed Hierarchical NiCo₂O₄-C@Ni(OH)₂ Core-Shell Nanofibers for High Performance Supercapacitors. *Carbon N. Y.* **2019**, *152*, 652–660. [CrossRef]
58. Abbas, Q.; Khurshid, H.; Yoosuf, R.; Lawrence, J.; Issa, B.A.; Abdelkareem, M.A.; Olabi, A.G. Engineering of Nickel, Cobalt Oxides and Nickel/Cobalt Binary Oxides by Electrodeposition and Application as Binder Free Electrodes in Supercapacitors. *Sci. Rep.* **2023**, *13*, 15654. [CrossRef] [PubMed]

59. Patake, V.D.; Joshi, S.S.; Lokhande, C.D.; Joo, O.S. Electrodeposited Porous and Amorphous Copper Oxide Film for Application in Supercapacitor. *Mater. Chem. Phys.* **2009**, *114*, 6–9. [[CrossRef](#)]
60. Chen, Y.; Guan, J.H.; Gan, H.; Chen, B.Z.; Shi, X.C. Electrochemical Growth of α -MnO₂ on Carbon Fibers for High-Performance Binder-Free Electrodes of Supercapacitors. *J. Appl. Electrochem.* **2018**, *48*, 105–113. [[CrossRef](#)]
61. Chou, S.L.; Wang, J.Z.; Chew, S.Y.; Liu, H.K.; Dou, S.X. Electrodeposition of MnO₂ Nanowires on Carbon Nanotube Paper as Free-Standing, Flexible Electrode for Supercapacitors. *Electrochem. Commun.* **2008**, *10*, 1724–1727. [[CrossRef](#)]
62. Velayutham, R.; Manikandan, R.; Raj, C.J.; Kale, A.M.; Kaya, C.; Palanisamy, K.; Kim, B.C. Electrodeposition of Vanadium Pentoxide on Carbon Fiber Cloth as a Binder-Free Electrode for High-Performance Asymmetric Supercapacitor. *J. Alloys Compd.* **2021**, *863*, 158332. [[CrossRef](#)]
63. Zhang, J.; Yi, X.-B.; Wang, X.C.; Ma, J.; Liu, S.; Wang, X.J. Nickel Oxide Grown on Carbon Nanotubes/Carbon Fiber Paper by Electrodeposition as Flexible Electrode for High-Performance Supercapacitors. *J. Mater. Sci. Mater. Electron.* **2015**, *26*, 7901–7908. [[CrossRef](#)]
64. Sahoo, S.; Naik, K.K.; Rout, C.S. Electrodeposition of Spinel MnCo₂O₄ Nanosheets for Supercapacitor Applications. *Nanotechnology* **2015**, *26*, 455401. [[CrossRef](#)] [[PubMed](#)]
65. Zhao, P.; Wang, N.; Hu, W.; Komarneni, S. Anode Electrodeposition of 3D Mesoporous Fe₂O₃ Nanosheets on Carbon Fabric for Flexible Solid-State Asymmetric Supercapacitor. *Ceram. Int.* **2019**, *45*, 10420–10428. [[CrossRef](#)]
66. Kazemi, S.H.; Asghari, A.; Kiani, M.A. High Performance Supercapacitors Based on the Electrodeposited Co₃O₄ Nanoflakes on Electro-Etched Carbon Fibers. *Electrochim. Acta* **2014**, *138*, 9–14. [[CrossRef](#)]
67. Danks, A.E.; Hall, S.R.; Schnepf, Z. The Evolution of “sol-Gel” Chemistry as a Technique for Materials Synthesis. *Mater. Horizons* **2016**, *3*, 91–112. [[CrossRef](#)]
68. Parashar, M.; Shukla, V.K.; Singh, R. Metal Oxides Nanoparticles via Sol-Gel Method: A Review on Synthesis, Characterization and Applications. *J. Mater. Sci. Mater. Electron.* **2020**, *31*, 3729–3749. [[CrossRef](#)]
69. Sankar Devi, V.; Athika, M.; Duraisamy, E.; Prasath, A.; Selva Sharma, A.; Elumalai, P. Facile Sol-Gel Derived Nanostructured Spinel Co₃O₄ as Electrode Material for High-Performance Supercapattery and Lithium-Ion Storage. *J. Energy Storage* **2019**, *25*, 100815. [[CrossRef](#)]
70. Wu, Y.Q.; Chen, X.Y.; Ji, P.T.; Zhou, Q.Q. Sol-Gel Approach for Controllable Synthesis and Electrochemical Properties of NiCo₂O₄ Crystals as Electrode Materials for Application in Supercapacitors. *Electrochim. Acta* **2011**, *56*, 7517–7522. [[CrossRef](#)]
71. Hu, G.; Tang, C.; Li, C.; Li, H.; Wang, Y.; Gong, H. The Sol-Gel-Derived Nickel-Cobalt Oxides with High Supercapacitor Performances. *J. Electrochem. Soc.* **2011**, *158*, A695–A699. [[CrossRef](#)]
72. Lobo, L.S.; Kalainathan, S.; Kumar, A.R. Investigation of Electrical Studies of Spinel FeCo₂O₄ Synthesized by Sol-Gel Method. *Superlattices Microstruct.* **2015**, *88*, 116–126. [[CrossRef](#)]
73. Tang, W.; Shan, X.; Li, S.; Liu, H.; Wu, X.; Chen, Y. Sol-Gel Process for the Synthesis of Ultrafine MnO₂ Nanowires and Nanorods. *Mater. Lett.* **2014**, *132*, 317–321. [[CrossRef](#)]
74. Wang, N.; Zhang, Q.; Zhao, P.; Yao, M.; Hu, W.; Komarneni, S. Highly Mesoporous LaNiO₃/NiO Composite with High Specific Surface Area as a Battery-Type Electrode. *Ceram. Int.* **2017**, *43*, 5687–5692. [[CrossRef](#)]
75. Thangavel, R.; Ganesan, B.K.; Thangavel, V.; Yoon, W.S.; Lee, Y.S. Emerging Materials for Sodium-Ion Hybrid Capacitors: A Brief Review. *ACS Appl. Energy Mater.* **2021**, *4*, 13376–13394. [[CrossRef](#)]
76. Zhu, G.N.; Wang, Y.G.; Xia, Y.Y. Ti-Based Compounds as Anode Materials for Li-Ion Batteries. *Energy Environ. Sci.* **2012**, *5*, 6652–6667. [[CrossRef](#)]
77. Ma, Y.; Wang, X.; Jia, Y.; Chen, X.; Han, H.; Li, C. Titanium Dioxide-Based Nanomaterials for Photocatalytic Fuel Generations. *Chem. Rev.* **2014**, *114*, 9987–10043. [[CrossRef](#)]
78. Aravindan, V.; Shubha, N.; Chui Ling, W.; Madhavi, S. Constructing High Energy Density Non-Aqueous Li-Ion Capacitors Using Monoclinic TiO₂-B Nanorods as Insertion Host. *J. Mater. Chem. A* **2013**, *1*, 6145–6151. [[CrossRef](#)]
79. Liu, H.; Bi, Z.; Sun, X.G.; Unocic, R.R.; Paranthaman, M.P.; Dai, S.; Brown, G.M. Mesoporous TiO₂-B Microspheres with Superior Rate Performance for Lithium Ion Batteries. *Adv. Mater.* **2011**, *23*, 3450–3454. [[CrossRef](#)]
80. Wang, Q.; Wen, Z.; Li, J. A Hybrid Supercapacitor Fabricated with a Carbon Nanotube Cathode and a TiO₂-B Nanowire Anode. *Adv. Funct. Mater.* **2006**, *16*, 2141–2146. [[CrossRef](#)]
81. Kim, H.; Cho, M.Y.; Kim, M.H.; Park, K.Y.; Gwon, H.; Lee, Y.; Roh, K.C.; Kang, K. A Novel High-Energy Hybrid Supercapacitor with an Anatase TiO₂-Reduced Graphene Oxide Anode and an Activated Carbon Cathode. *Adv. Energy Mater.* **2013**, *3*, 1500–1506. [[CrossRef](#)]
82. Ramasubbu, V.; Omar, F.S.; Ramesh, K.; Ramesh, S.; Shajan, X.S. Three-Dimensional Hierarchical Nanostructured Porous TiO₂ Aerogel/Cobalt Based Metal-Organic Framework (MOF) Composite as an Electrode Material for Supercapattery. *J. Energy Storage* **2020**, *32*, 101750. [[CrossRef](#)]
83. Ohzuku, T.; Ueda, A.; Yamamoto, N. Zero-Strain Insertion Material of Li [Li_{1/3}Ti_{5/3}]O₄ for Rechargeable Lithium Cells. *J. Electrochem. Soc.* **1995**, *142*, 1431–1435. [[CrossRef](#)]

84. Li, X.; Qu, M.; Yu, Z. Structural and Electrochemical Performances of $\text{Li}_4\text{Ti}_{5-x}\text{Zr}_x\text{O}_{12}$ as Anode Material for Lithium-Ion Batteries. *J. Alloys Compd.* **2009**, *487*, 12–17. [[CrossRef](#)]
85. Khairy, M.; Bayoumy, W.A.; Qasim, K.F.; El-Shereafy, E.; Mousa, M.A. Ternary V-Doped $\text{Li}_4\text{Ti}_5\text{O}_{12}$ -Polyaniline-Graphene Nanostructure with Enhanced Electrochemical Capacitance Performance. *Mater. Sci. Eng. B* **2021**, *271*, 115312. [[CrossRef](#)]
86. Naoi, K.; Naoi, W.; Aoyagi, S.; Miyamoto, J.I.; Kamino, T. New Generation “Nanohybrid Supercapacitor”. *Acc. Chem. Res.* **2013**, *46*, 1075–1083. [[CrossRef](#)] [[PubMed](#)]
87. Lee, B.; Yoon, J.R. Preparation and Characteristics of $\text{Li}_4\text{Ti}_5\text{O}_{12}$ with Various Dopants as Anode Electrode for Hybrid Supercapacitor. *Curr. Appl. Phys.* **2013**, *13*, 1350–1353. [[CrossRef](#)]
88. Naoi, K.; Ishimoto, S.; Isobe, Y.; Aoyagi, S. High-Rate Nano-Crystalline $\text{Li}_4\text{Ti}_5\text{O}_{12}$ Attached on Carbon Nano-Fibers for Hybrid Supercapacitors. *J. Power Sources* **2010**, *195*, 6250–6254. [[CrossRef](#)]
89. Jeong, J.H.; Lee, G.W.; Kim, Y.H.; Choi, Y.J.; Roh, K.C.; Kim, K.B. A Holey Graphene-Based Hybrid Supercapacitor. *Chem. Eng. J.* **2019**, *378*, 122126. [[CrossRef](#)]
90. Choi, H.S.; Im, J.H.; Kim, T.; Park, J.H.; Park, C.R. Advanced Energy Storage Device: A Hybrid BatCap System Consisting of Battery-Supercapacitor Hybrid Electrodes Based on $\text{Li}_4\text{Ti}_5\text{O}_{12}$ -Activated-Carbon Hybrid Nanotubes. *J. Mater. Chem.* **2012**, *22*, 16986–16993. [[CrossRef](#)]
91. Jung, H.G.; Venugopal, N.; Scrosati, B.; Sun, Y.K. A High Energy and Power Density Hybrid Supercapacitor Based on an Advanced Carbon-Coated $\text{Li}_4\text{Ti}_5\text{O}_{12}$ Electrode. *J. Power Sources* **2013**, *221*, 266–271. [[CrossRef](#)]
92. Kim, H.; Park, K.Y.; Cho, M.Y.; Kim, M.H.; Hong, J.; Jung, S.K.; Roh, K.C.; Kang, K. High-Performance Hybrid Supercapacitor Based on Graphene-Wrapped $\text{Li}_4\text{Ti}_5\text{O}_{12}$ and Activated Carbon. *ChemElectroChem* **2014**, *1*, 125–130. [[CrossRef](#)]
93. Manthiram, A. A Reflection on Lithium-Ion Battery Cathode Chemistry. *Nat. Commun.* **2020**, *11*, 1–9. [[CrossRef](#)]
94. Godillot, G.; Taberna, P.L.; Daffos, B.; Simon, P.; Delmas, C.; Guerlou-Demouragues, L. High Power Density Aqueous Hybrid Supercapacitor Combining Activated Carbon and Highly Conductive Spinel Cobalt Oxide. *J. Power Sources* **2016**, *331*, 277–284. [[CrossRef](#)]
95. Numan, A.; Khalid, M.; Ramesh, S.; Ramesh, K.; Shamsudin, E.M.; Zhan, Y.; Jagadesh, P. Facile Sonochemical Synthesis of 2D Porous Co_3O_4 Nanoflake for Supercapattery. *J. Alloys Compd.* **2020**, *819*, 153019. [[CrossRef](#)]
96. Sivakumar, P.; Jana, M.; Kota, M.; Jung, M.G.; Gedanken, A.; Park, H.S. Controllable Synthesis of Nanohorn-like Architectured Cobalt Oxide for Hybrid Supercapacitor Application. *J. Power Sources* **2018**, *402*, 147–156. [[CrossRef](#)]
97. Vattikuti, S.V.P.; Hoang Ngoc, C.T.; Nguyen, H.; Nguyen Thi, N.H.; Shim, J.; Dang, N.N. Carbon Nitride Coupled Co_3O_4 : A Pyrolysis-Based Approach for High-Performance Hybrid Energy Storage. *J. Phys. Chem. Lett.* **2023**, *14*, 9412–9423. [[CrossRef](#)]
98. Arjunan, A.; Ramasamy, S.; Kim, J.; Kim, S.K. Co_3O_4 Nanoparticles-Embedded Nitrogen-Doped Porous Carbon Spheres for High-Energy Hybrid Supercapacitor Electrodes. *J. Energy Storage* **2023**, *68*, 107758. [[CrossRef](#)]
99. Hosseinzadeh, B.; Nagar, B.; Benages-Vilau, R.; Gomez-Romero, P.; Kazemi, S.H. MOF-Derived Conformal Cobalt Oxide/C Composite Material as High-Performance Electrode in Hybrid Supercapacitors. *Electrochim. Acta* **2021**, *389*, 138657. [[CrossRef](#)]
100. Sahoo, S.; Milton, A.; Sood, A.; Kumar, R.; Choi, S.; Maity, C.K.; Han, S.S. Microwave-Assisted Synthesis of Perovskite Hydroxide-Derived $\text{Co}_3\text{O}_4/\text{SnO}_2$ /Reduced Graphene Oxide Nanocomposites for Advanced Hybrid Supercapacitor Devices. *J. Energy Storage* **2024**, *99*, 113321. [[CrossRef](#)]
101. Muralee Gopi, C.V.V.; Vinodh, R.; Sambasivam, S.; Obaidat, I.M.; Naidu Kalla, R.M.; Kim, H.J. One-Pot Synthesis of Copper Oxide–Cobalt Oxide Core–Shell Nanocactus-like Heterostructures as Binder-Free Electrode Materials for High-Rate Hybrid Supercapacitors. *Mater. Today Energy* **2019**, *14*, 100358. [[CrossRef](#)]
102. Izwan Misnon, I.; Krishnan, S.G.; Jose, R. Thin Chemisorbed Polyaniline Film on Cobalt Oxide as an Electrode for Hybrid Energy Storage Devices. *ChemistrySelect* **2020**, *5*, 7973–7983. [[CrossRef](#)]
103. Chen, H.; Bao, E.; Du, X.; Ren, X.; Liu, X.; Li, Y.; Xu, C. Advanced Hybrid Supercapacitors Assembled with High-Performance Porous $\text{MnCo}_2\text{O}_{4.5}$ Nanosheets as Battery-Type Cathode Materials. *Colloids Surfaces A Physicochem. Eng. Asp.* **2023**, *657*, 130663. [[CrossRef](#)]
104. Li, W.; Xu, K.; Song, G.; Zhou, X.; Zou, R.; Yang, J.; Chen, Z.; Hu, J. Facile Synthesis of Porous $\text{MnCo}_2\text{O}_{4.5}$ Hierarchical Architectures for High-Rate Supercapacitors. *CrystEngComm* **2014**, *16*, 2335–2339. [[CrossRef](#)]
105. Liu, Y.; Du, X.; Li, Y.; Bao, E.; Ren, X.; Chen, H.; Tian, X.; Xu, C. Nanosheet-Assembled Porous $\text{MnCo}_2\text{O}_{4.5}$ Microflowers as Electrode Material for Hybrid Supercapacitors and Lithium-Ion Batteries. *J. Colloid Interface Sci.* **2022**, *627*, 815–826. [[CrossRef](#)]
106. Yang, C.H.; Chen, Y.C.; Wu, C.F.; Chung, R.J.; Yougbaré, S.; Lin, L.Y. Novel Synthesis of ZIF67-Derived MnCo_2O_4 Nanotubes Using Electrospinning and Hydrothermal Techniques for Supercapacitor. *J. Solid State Chem.* **2022**, *313*, 123351. [[CrossRef](#)]
107. Che, H.; Wang, Y.; Mao, Y. Novel Flower-like MnCo_2O_4 Microstructure Self-Assembled by Ultrathin Nanoflakes on the Microspheres for High-Performance Supercapacitors. *J. Alloys Compd.* **2016**, *680*, 586–594. [[CrossRef](#)]
108. Gao, Y.; Xia, Y.; Wan, H.; Xu, X.; Jiang, S. Enhanced Cycle Performance of Hierarchical Porous Sphere MnCo_2O_4 for Asymmetric Supercapacitors. *Electrochim. Acta* **2019**, *301*, 294–303. [[CrossRef](#)]

109. Ahmad, A.; Khan, S.; Javed, M.S.; Osman, S.; Li, H.; Majeed, S.; Luque, R. Improved Electrochemical Performance of Aqueous Hybrid Supercapacitors Using CrCo_2O_4 Mesoporous Nanowires: An Innovative Strategy toward Sustainable Energy Devices. *ACS Appl. Mater. Interfaces* **2024**, *16*, 6920–6930. [[CrossRef](#)]
110. Sivakumar, P.; Kulandaivel, L.; Park, J.W.; Raj, C.J.; Savariraj, A.D.; Manikandan, R.; Rajendran, R.; Jung, H. Electroactive Site Enriched Battery-Type Worm-like Cobalt Tungstate Nanoarchitecture Electrode Material for Performance-Enhanced Hybrid Supercapacitor. *Surf. Interfaces* **2023**, *40*, 103111. [[CrossRef](#)]
111. Zhao, Y.; Zheng, J.; Yuan, M.; Wang, Y.; Liu, W.; Yang, S.; Li, G.; Lian, J.; Bu, Y. Boosting the Energy Density of Iron-Cobalt Oxide Based Hybrid Supercapacitors by Redox-Additive Electrolytes. *J. Alloys Compd.* **2021**, *885*, 160886. [[CrossRef](#)]
112. Nagaraju, M.; Ramulu, B.; Girija Shankar, E.; Su Yu, J. Rational Design of Hierarchical Zeolitic Imidazolate Framework-67@ Cu_2CoO_3 Core-Shell Architectures for Hybrid Supercapacitor Applications. *Appl. Surf. Sci.* **2023**, *640*, 158339. [[CrossRef](#)]
113. Srivastav, S.; Paliwal, M.K.; Meher, S.K. Ribbon-like Nickel Cobaltite with Layer-by-Layer-Assembled Ordered Nanocrystallites for Next-Generation All-Solid-State Hybrid Supercapacitors. *Langmuir* **2022**, *38*, 3969–3983. [[CrossRef](#)]
114. Ganesan, M.; Alagar, S.; Bagchi, V.; Piraman, S. Surface Oxygen Engineered ZnCo_2O_4 Planar Hybrid Supercapacitor Electrode for High Energy Applications. *J. Energy Storage* **2024**, *98*, 112954. [[CrossRef](#)]
115. Zhang, S.; Tan, H.; Rui, X.; Yu, Y. Vanadium-Based Materials: Next Generation Electrodes Powering the Battery Revolution? *Acc. Chem. Res.* **2020**, *53*, 1660–1671. [[CrossRef](#)] [[PubMed](#)]
116. Tang, H.; Peng, Z.; Wu, L.; Xiong, F.; Pei, C.; An, Q.; Mai, L. Vanadium-Based Cathode Materials for Rechargeable Multivalent Batteries: Challenges and Opportunities. *Electrochem. Energy Rev.* **2018**, *1*, 169–199. [[CrossRef](#)]
117. Yan, Y.; Li, B.; Guo, W.; Pang, H.; Xue, H. Vanadium Based Materials as Electrode Materials for High-Performance Supercapacitors. *J. Power Sources* **2016**, *329*, 148–169. [[CrossRef](#)]
118. Yue, Y.; Liang, H. Micro- and Nano-Structured Vanadium Pentoxide (V_2O_5) for Electrodes of Lithium-Ion Batteries. *Adv. Energy Mater.* **2017**, *7*, 1–32. [[CrossRef](#)]
119. Yang, Y.; Tang, Y.; Fang, G.; Shan, L.; Guo, J.; Zhang, W.; Wang, C.; Wang, L.; Zhou, J.; Liang, S. Li^+ Intercalated V_2O_5 : $\text{N H}_2\text{O}$ with Enlarged Layer Spacing and Fast Ion Diffusion as an Aqueous Zinc-Ion Battery Cathode. *Energy Environ. Sci.* **2018**, *11*, 3157–3162. [[CrossRef](#)]
120. Liu, M.; Su, B.; Tang, Y.; Jiang, X.; Yu, A. Recent Advances in Nanostructured Vanadium Oxides and Composites for Energy Conversion. *Adv. Energy Mater.* **2017**, *7*, 1700885. [[CrossRef](#)]
121. Xu, Y.; Yang, X.; Li, X.; Gao, Y.; Wang, L.; Lü, W. Flexible Zinc-Ion Hybrid Supercapacitor Based on Co^{2+} -Doped Polyaniline/ V_2O_5 Electrode. *J. Power Sources* **2024**, *623*, 235399. [[CrossRef](#)]
122. Keum, K.; Park, D.; Park, M.; Lee, Y.; Lee, H.; Jeong, H.; Kim, J.W.; Kim, D.-w.; Ha, J.S. All Vanadium-Based Li-Ion Hybrid Supercapacitor with Enhanced Electrochemical Performance via Prelithiation. *J. Alloys Compd.* **2022**, *914*, 165288. [[CrossRef](#)]
123. Jing, X.; Zhang, Y.; Jiang, H.; Cheng, Y.; Xing, N.; Meng, C. Facile Template-Free Fabrication of Hierarchical V_2O_5 Hollow Spheres with Excellent Charge Storage Performance for Symmetric and Hybrid Supercapacitor Devices. *J. Alloys Compd.* **2018**, *763*, 180–191. [[CrossRef](#)]
124. Aravindan, V.; Cheah, Y.L.; Mak, W.F.; Wee, G.; Chowdari, B.V.R.; Madhavi, S. Fabrication of High Energy-Density Hybrid Supercapacitors Using Electrospun V_2O_5 Nanofibers with a Self-Supported Carbon Nanotube Network. *Chempluschem* **2012**, *77*, 570–575. [[CrossRef](#)]
125. Vishwakarma, N.; Mashangva, T.T.; Rajput, S.; Pham, T.D.; Kumar, M.; Sharma, A. Unlocking the Potential for Revolutionary Energy Storage Capabilities of $\text{V}_2\text{O}_5/\text{GO}$ Nanocomposites Synthesized under Microwave Irradiation. *J. Energy Storage* **2024**, *103*, 114405. [[CrossRef](#)]
126. Wang, G.; Ding, Y.; Xu, Z.; Wang, G.; Li, Z.; Yan, Z. $\text{Co}_3\text{O}_4@\text{Mn-Ni(OH)}_2$ Core–Shell Heterostructure for Hybrid Supercapacitor Electrode with High Utilization. *Chem. Eng. J.* **2023**, *469*, 143984. [[CrossRef](#)]
127. Arun Kumar, S.; Sarasamreen, I.; Balaji, C.; Gowdhaman, A.; Ramesh, R.; Anbarasan, P.M. Elevates the Electrochemical Stability Performance of Hydrothermally Synthesized Co_3O_4 Nanowires/NF for Hybrid Supercapacitors. *Inorg. Chem. Commun.* **2023**, *158*, 111506. [[CrossRef](#)]
128. Chen, H.; Du, X.; Sun, J.; Wu, R.; Wang, Y.; Xu, C. Template-Free Synthesis of Novel Co_3O_4 Micro-Bundles Assembled with Flakes for High-Performance Hybrid Supercapacitors. *Ceram. Int.* **2021**, *47*, 716–724. [[CrossRef](#)]
129. Iqbal, M.Z.; Shaheen, M.; Aftab, U.; Ahmad, Z.; Solangi, M.Y.; Abro, M.I.; Wabaidur, S.M. Faradically Dominant Pseudocapacitive Manganese Cobalt Oxide Electrode Materials for Hybrid Supercapacitors and Electrochemical Water Splitting. *Energy Fuels* **2024**, *38*, 2416–2425. [[CrossRef](#)]
130. Reghunath, B.S.; Sunaja Devi, K.R.; Rajasekaran, S.; Saravanakumar, B.; William, J.J.; Pinheiro, D. CoFe_2O_4 Nanoparticles Embedded 2D Cr_2CTx MXene: A New Material for Battery like Hybrid Supercapacitors and Oxygen Evolution Reaction. *J. Energy Storage* **2024**, *84*, 110775. [[CrossRef](#)]
131. Bhagwan, J.; Han, J.I. Formation of MWCNT/Li Co_2O_4 Nanoplates and Their Application for Hybrid Supercapacitor. *Ceram. Int.* **2024**, *50*, 10676–10687. [[CrossRef](#)]

132. Zhao, L.; Zhang, H.; Ma, B. Formation of Carbon-Incorporated NiO@Co₃O₄ Nanostructures via a Direct Calcination Method and Their Application as Battery-Type Electrodes for Hybrid Supercapacitors. *ACS Omega* **2023**, *8*, 10503–10511. [[CrossRef](#)]
133. Bhosale, R.; Bhosale, S.; Chavan, V.; Jambhale, C.; Kim, D.K.; Kolekar, S. Hybrid Supercapacitors Based on Nanoporous Carbon and CoFe₂O₄ Derived from a Bimetallic Organic Framework. *ACS Appl. Nano Mater.* **2024**, *7*, 2244–2257. [[CrossRef](#)]
134. Govindasamy, T.; Mathew, N.K.; Asapu, V.K.; Subramanian, V.; Subramanian, B. Modulating the Structural and Magnetic Properties of Fe₃O₄ NPs for High-Performance Supercapattery and EMI Shielding Applications. *J. Energy Storage* **2024**, *79*, 110243. [[CrossRef](#)]
135. Huang, H.; Wang, X.; Tervoort, E.; Zeng, G.; Liu, T.; Chen, X.; Sologubenko, A.; Niederberger, M. Nano-Sized Structurally Disordered Metal Oxide Composite Aerogels as High-Power Anodes in Hybrid Supercapacitors. *ACS Nano* **2018**, *12*, 2753–2763. [[CrossRef](#)] [[PubMed](#)]
136. Shen, L.; Lv, H.; Chen, S.; Kopold, P.; van Aken, P.A.; Wu, X.; Maier, J.; Yu, Y. Peapod-like Li₃VO₄/N-Doped Carbon Nanowires with Pseudocapacitive Properties as Advanced Materials for High-Energy Lithium-Ion Capacitors. *Adv. Mater.* **2017**, *29*, 1–8. [[CrossRef](#)] [[PubMed](#)]
137. Lim, E.; Lim, W.G.; Jo, C.; Chun, J.; Kim, M.H.; Roh, K.C.; Lee, J. Rational Design of Li₃VO₄@carbon Core-Shell Nanoparticles as Li-Ion Hybrid Supercapacitor Anode Materials. *J. Mater. Chem. A* **2017**, *5*, 20969–20977. [[CrossRef](#)]
138. Zhou, Y.; Wen, L.L.; Zhan, K.; Yan, Y.; Zhao, B. Three-Dimensional Porous Graphene/Nickel Cobalt Mixed Oxide Composites for High-Performance Hybrid Supercapacitor. *Ceram. Int.* **2018**, *44*, 21848–21854. [[CrossRef](#)]
139. Hao, Y.; Guo, H.; Ren, H.; Yang, Z.; Peng, L.; Liu, Y.; Yang, W. Highly Dispersive Nickel Vanadium Oxide Nanoparticles Anchored on Nickel Cobalt Phosphate Micron-Sheets as Cathodes for High-Energy Hybrid Supercapacitor Devices. *J. Alloys Compd.* **2025**, *1010*, 177893. [[CrossRef](#)]
140. Sun, H.; Miao, Y.; Wang, G.; Han, X.; Xu, C.; Zhu, J.; Chen, H. Battery-Type ZnCo₂O₄ Nanosheets and Nanowires as Advanced Cathode Materials for Hybrid Supercapacitors with Ultra-Long Cycling Stability. *J. Energy Storage* **2024**, *92*, 112189. [[CrossRef](#)]
141. Kour, S.; Kour, P.; Sharma, A.L. A Chromium Cobaltite Based Ternary Composite as an Efficient Electrode Material for Hybrid Supercapacitors with Theoretical Investigation. *Nanoscale* **2024**, *16*, 21456–21470. [[CrossRef](#)]
142. Suganya, S.; Kousi, F.; Sambasivam, S.; Tighezza, A.M.; Velsankar, K.; Sudhahar, S. Investigations of Ternary Cu-Mn-Zn Oxide Nanocomposites as Potential Electrode for Hybrid Supercapacitors by One-Pot Hydrothermal Method. *J. Energy Storage* **2025**, *109*, 115181. [[CrossRef](#)]
143. Fei, T.; Ahmad, T.; Usman, M.; Ahmad, A.; Saleem, A.; Hanif, M.B.; Karami, A.M.; Javed, M.S.; Akkinepally, B.; Xia, C. Zn-Doped Cr₂O₃ Oxides Boosted the Electrochemical Performance of Aqueous Hybrid Supercapacitor. *Electrochim. Acta* **2024**, *476*, 143673. [[CrossRef](#)]
144. Zheng, J.; Meng, D.; Guo, J.; Liu, X.; Zhou, L.; Wang, Z. Defect Engineering for Enhanced Electrocatalytic Oxygen Reaction on Transition Metal Oxides: The Role of Metal Defects. *Adv. Mater.* **2024**, *36*, e2405129. [[CrossRef](#)] [[PubMed](#)]
145. Sun, Y.; Wu, T.; Bao, Z.; Moon, J.; Huang, Z.; Chen, Z.; Chen, H.; Li, M.; Yang, Z.; Chi, M.; et al. Defect Engineering of Ceria Nanocrystals for Enhanced Catalysis via a High-Entropy Oxide Strategy. *ACS Cent. Sci.* **2022**, *8*, 1081–1090. [[CrossRef](#)] [[PubMed](#)]
146. Choi, J.; Im, S.; Choi, J.; Surendran, S.; Moon, D.J.; Kim, J.Y.; Kim, J.K.; Sim, U. Recent Advances in 2D Structured Materials with Defect-Exploiting Design Strategies for Electrocatalysis of Nitrate to Ammonia. *Energy Mater.* **2024**, *4*, 400020. [[CrossRef](#)]
147. Lu, W.; Yan, L.; Ye, W.; Ning, J.; Zhong, Y.; Hu, Y. Defect Engineering of Electrode Materials towards Superior Reaction Kinetics for High-Performance Supercapacitors. *J. Mater. Chem. A* **2022**, *10*, 15267–15296. [[CrossRef](#)]

Disclaimer/Publisher’s Note: The statements, opinions and data contained in all publications are solely those of the individual author(s) and contributor(s) and not of MDPI and/or the editor(s). MDPI and/or the editor(s) disclaim responsibility for any injury to people or property resulting from any ideas, methods, instructions or products referred to in the content.